# POLITECNICO DI TORINO

**MSc. Environmental and Land Engineering**

**Academic Year 2023/24**

# High-Density LiDAR Data Analysis for Urban Flood Assessment


**Supervisors**
Prof. Boccardo Piero
Prof. Laio Francesco

**Candidate**
Angeliki Makellaraki

# Abstract

Urban areas are facing growing challenges associated with climate change, necessitating the adoption of advanced tools such as Lidar technology and Geographic Information System (GIS) to effectively assess and mitigate these issues. The aim of this study focuses on the use of such tools to generate high-resolution terrain representations, including Digital Terrain Models (DTM) and Digital Surface Models (DSM), and to conduct a comprehensive hydrological analysis of the Meisino Park in Turin, Italy, an area historically susceptible to flooding events. Lidar data, provided by the SDG11LAB laboratory of the Polytechnic School of Turin (DIST), have been used to produce precise digital elevation models by capturing elevation data for thousands of points across the terrain, enabling highly accurate analysis, *1m/pixel*. Given that Lidar instrument cannot penetrate the water surface, supplementary data of the river area have been collected from different sources to obtain a complete digital elevation model. As a result, the first focus of the study is the statistical validation of the terrain models obtained. Statistical measures such as Root Mean Square Error (RMSE) and Normalized Median Absolute Deviation (NMAD) have been used to ensure the accuracy of the results obtained. An additional analysis has been conducted to extract urban features present in the terrain model, such as buildings and roads. These data have been extracted from both Lidar points and online databases, such as the Geoportal website of the Piedmont region. The ultimate refinement of feature extraction has been achieved by conducting a supervised classification process using ENVI software.

The final step of this thesis is focused on the hydrological analysis, which encompasses the generation of hydrographic basins of a subset of the area under study using the DTM with the highest accuracy obtained. Various precipitation scenarios, ranging from low-intensity rainfall (2 mm/h) to extreme events (200 mm/h), are considered to evaluate the area's hydrological response under different climatic conditions. Additionally, the study examines the impact of varying street inlet clogging conditions on discharge calculations for each sub catchment, highlighting specific street inlets that are particularly susceptible to inundation across different precipitation and clogging scenarios. The findings of this study will reveal a notable increase in surface flow when higher number of street inlets are clogged, and higher precipitation intensity scenarios are considered.

# Table of Contents

# List of Figures

# List of Tables



# Abbreviations

| | |
|---|---|
| DTM | Digital Terrain Model |
| DSM | Digital Surface Model |
| LiDAR | Light Detection and Ranging |
| AOI | Area of Interest |
| ME | Ministry of the Environment |
| ROI | Region of Interest |
| TWI | Topographic wetness index |
| IPCC | Intergovernmental Panel on Climate Change |

# 1. Introduction

In recent years, the impacts of changing climate patterns have emerged as a significant concern for urban areas worldwide. Events such as intensified rainfall and extreme heatwaves have notably affected densely populated regions. Italy, in particular, faces a significant flood challenge, with nearly 10% of its land vulnerable to this threat. A report by the Ministry of the Environment and Land Protection indicates that 2.6% of Italy's territory is at high risk of flooding, and notably, 30% of flood-prone regions include residential areas located in floodplains, putting approximately 3.5 million people, or 6% of the population, at risk[1].

In the context of climate change, studying pluvial flooding events becomes crucial as they occur following episodes of high-intensity rainfall. Pluvial flooding arises when surface runoff cannot be effectively managed by underground drainage systems, resulting in overflow onto the surface. The Intergovernmental Panel on Climate Change (IPCC) predicts that extreme weather events associated with climate change will become more frequent, impacting both the intensity and frequency of rainfall events[2].

Due to these reasons, there is an emerging need for urban flood assessment and risk management strategies, necessitating the use of innovative and advanced tools. To address this pressing issue, this thesis investigates the importance of high-resolution digital terrain representations, particularly Digital Elevation Models (DEMs). These models are essential for understanding the complex topography of urban areas and accurately assessing flood risks.

DEMs can be generated through various methods, including ground surveys, aerial surveys, or remote sensing techniques like LiDAR (Light Detection and Ranging). While LiDAR offers very high precision and accuracy in terrain mapping, it faces limitations such as its inability to penetrate water surfaces and the potential high costs associated with the necessary instruments. Nonetheless, its ability to penetrate vegetation and minimize scattering makes it invaluable in creating high-quality Digital Terrain Models (DTMs) and Digital Surface Models (DSMs)[3].

These digital terrain models play a crucial role in delineating watershed boundaries and identifying drainage patterns. However, in urban areas, this analysis is complicated by the presence of man-made features such as streets and buildings. These features significantly influence the runoff coefficient of each sub catchment, adding complexity to flood risk assessments and management strategies. Therefore, understanding the interplay between natural topography and urban infrastructure is essential in calculating the overland flow distribution and for developing effective flood mitigation measures.

## 1.1 Objectives of the study

The aim of this study is to emphasise the significance of Remote Sensing and GIS techniques in urban hydrological analysis. This is achieved by:

- Conducting a statistical analysis in order to obtain the most accurate DTM representing the AOI.
- Extracting key features from LiDAR point cloud data using ENVI LiDAR. These features are fundamental input for the flood assessment process.
- Conducting a supervised classification of the study area using ENVI software to improve the classification of missing points.
- Utilizing ArcGIS Pro to delineate sub catchments based on the street inlets present in the area and develop a simplified hydrological model.
- Analyse the feasibility of the sub catchments obtained under different precipitation and clogging scenarios.

The study will account for real-world scenarios where street inlets may be blocked for different reasons, such as poor maintenance. Hence, three distinct occlusion scenarios—0%, 10%, and 50%—will be considered.

## 1.2 Site Characterisation

The study area is located in the eastern part of Turin, near Meisino Park. Turin itself is situated in the northwest region of Italy, specifically in Piedmont region. Figures 1 and 2 illustrate the geographical location of Turin, as well as the specific area under investigation. Covering approximately 8 $km^2$, the study area mainly consists of flat terrain, with the exception of hilly terrain in the southeast portion. This spatial domain is characterized by diverse land use patterns, such as infrastructure networks, natural features, and vegetated areas, all of which are important for the hydraulic modelling of the area.

The choice of this area arises from the recurring flooding issues experienced in the Meisino vicinity, primarily due to the nearby river, as it is located at the confluence of the Po River and the Stura River. The most recent recorded flood events occurred in 1994, 2000, and 2016[4]. Therefore, it is relevant to assess the adequacy of the existing drainage system in managing high surface flow occurrences. However, it's important to note that this study exclusively examines precipitation-induced flooding scenarios and not those caused by the water level rising of the river.

*Figure 1: City of Turin*

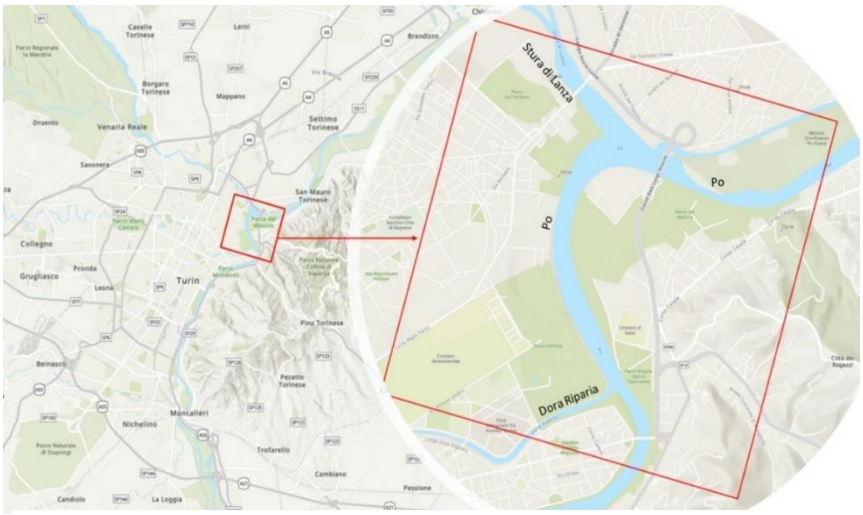


*Figure 2: City of Turin, zoom in the Area Of Interest*

# 2. State Of the Art

## 2.1 LiDAR Technology and DEM generation

LiDAR is an active remote sensing technology, that produces highly precise and dense elevation data. A LiDAR system deploys a laser scanner, which can be ground-based, mounted on aircraft (airborne LiDAR), or satellite-based. The mechanism involves emitting discrete laser pulses from the scanner, recording the time taken for these pulses to travel to ground targets, and subsequently calculating the distances between the emitter and the targets. In the case of airborne LiDAR systems, the setup typically

comprises three core components: a laser scanner unit, a Global Positioning System (GPS) receiver, and an Inertial Measurement Unit (IMU). These components work in concert to determine the laser's instantaneous position and orientation concerning the earth's surface, utilizing onboard GPS and Inertia Navigation System (INS). Additionally, supplementary information concerning the scan angle and a GPS base station is necessary to construct the three-dimensional position of ground features[5].

While LiDAR technology has proven to be highly efficient in various applications, including flood modelling, some limitations must be considered, especially when applied to river areas. LiDAR relies on laser pulses to measure distances, which can be blocked by water bodies due to their reflective properties (Figure 3). In river environments, the laser pulses encounter difficulties in penetrating the water surface and so measures regarding the riverbed elevation are not accurately calculated. For this reason, it was necessary to consider other data sources to extract elevation information on the Po, Dora Riparia and Stura di Lanzo watercourses.

*Figure 3:Spatial Distribution of LiDAR Data and Missing Points in the River Zone*

# 2.2 Digital Terrain Model Generation

The initial input data utilized for the processing was the LiDAR point cloud, which was generated from a survey conducted by the Polytechnic School of Turin in January 2022. The survey was focused on the entire area of the city of Turin. However, for this specific task, only the LiDAR data referred to the area of Meisino was considered. The cloud consists in 24,504,671.00 points in total and the data were distributed through 48 ".las" files. The information generated by the acquisition was very dense, representing buildings and infrastructure with high accuracy. It's essential to note that the LiDAR acquisition was nadiral, meaning it was collected from a vertically downward perspective.

To overcome the technical limitations of the LiDAR instrument over the river surface, various data sources accessible through the Italian national and regional data portals were explored. Initially, data obtained from the **Ministry of the Environment**, collected during a LiDAR survey in 2009 was examined. This dataset provided a more detailed representation of watercourses compared to the 2022 survey, and it included both the LiDAR point cloud and an already processed Digital Terrain Model (DTM) with a resolution of 1 meter per pixel, covering nearly the entire Area of Interest (AOI). Additionally, data from the **Po Basin Authority** (AdBPo) for the Po River was incorporated, which included DTMs with a resolution of 2 meters per pixel, generated from LiDAR acquisitions conducted in 2004-2005, with a specific focus on the watercourse. By merging these diverse data sources, it was possible to extract elevation information for the watercourses, particularly the Po, Dora Riparia, and Stura di Lanza. In this way an effective mitigation of the limitations encountered during the 2022 LiDAR acquisition was achieved.

Using different data sources, Digital Terrain Models (DTMs) were generated with varying levels of accuracy and resolution. To validate these DTMs and determine the most optimal one(s) for flood modelling input, high-precision elevation points were employed as reference data. These reference points were gathered from the Piedmont Regional Geoportal, which offers public access to various products acquired and processed over the years for the regional territory. Table 1 shows a summary of the different data sources utilized during the processing stages, along with specifications regarding their quality and the acquisition period:

| Data source | Available data | Acquisition period |
|---|---|---|
| *Ministry of the Environment (ME)* | LiDAR Point Clouds | 2009 |
| | DTM Turin 1 m/pixel | 2009 |
| *Polytechnic University of Turin (PoliTO)* | LiDAR Point Clouds | 2022 |
| *Po Basin Autority (AdBPo )* | DTM Po River 2 m/pixel | 2004-2005 |
| *Piedmont Region* | Elevation points | Update to 2016 |
| | Areal Hydrography | Update to 2016 |
| *Municipality of Turin* | Areal Hydrography | Update to 2023 |

*Table 1: Summary of dataset used for the analysis.*

# 2.3 Data Processing

In the initial phase, the previously mentioned LiDAR point cloud data acquired by the Polytechnic School of Turin, has been processed using ENVI LiDAR software. This

software, well-suited for its reliability in managing LiDAR point clouds, was chosen for its capabilities in creating very high-resolution DTMs. ENVI LiDAR offers various optimizations that enhance result accuracy. The LiDAR points were automatically registered based on their coordinates, utilizing the **WGS84-UTM 32N** reference system.

Key to this process is the automatic data classification (Figure 4), where the LiDAR point cloud is categorized into features like buildings, vegetation, and ground points. This classification enables the generation of specific feature representations. Additionally, point cloud density adjustments were made to reduce the number of points, aiding in eliminating outliers and uncertainties while reducing processing time. The resulting high-resolution DTM (**DTML, processed**) served as input for the next steps.

*Figure 4: ENVI LiDAR Classification: Class Colour Representation*

In the second part of our study, the objective was to integrate the urban information extracted from the processed DTM (**DTML, processed**) with other data sources that could accurately represent watercourses within the AOI. To do this, water masks had to be created to divide the urban areas from the rivers in the AOI. This was achieved by utilizing vector data related to areal hydrography, which was available in both the **Municipality of Turin** and the **Piedmont Region databases**. These datasets allowed the definition of the boundaries of the watercourses and subsequently create a mask that represented these river areas. Conversely, the remaining areas were considered urban, leading to the creation of a second mask that included these regions but excluded the watercourses. Once these masks were generated, they served as tools for extracting precise information from the DTMs. This process considered both the DTMs processed by ENVI LiDAR and the external DTMs.

The final step in this data processing phase involved merging the two extracted DTMs: one capturing the urban areas and the other representing the watercourses. Through this integration, the final high-resolution model (**$DTM_f$**) has been created, as a combination of several reliable sources. It's worth noting that the access to different datasets, allowed the exploration of various combinations of DTMs in order to determine the most suitable option for our analysis. The different DTMs combination are illustrated below:

| | **Urban section** | **Watercourse section** | **Final resolution** |
|---|---|---|---|
| **$DTM_f$ (1)** | $DTM_{L,\ processed}$ PoliTO | DTM AdBPo | 2 m/pixel |
| **$DTM_f$ (2)** | $DTM_{L,\ processed}$ PoliTO | $DTM_{available}$ ME | 1 m/pixel |
| **$DTM_f$ (3)** | $DTM_{L,\ processed}$ PoliTO | $DTM_{L,\ processed}$ ME | 1 m/pixel |
| **$DTM_f$ (4)** | $DTM_{L,\ processed}$ ME | $DTM_{L,\ processed}$ ME | 1 m/pixel |

*Table 2: Combination of urban and watercourse section extracted from different sources to generate the final $DTM_f$.*

Figure 5 and Figure 6 provide a visual representation of the four distinct $DTM_f$ models resulting from the combination of various datasets. While these models may appear quite similar at first glance, they exhibit variations in coloration corresponding to the specific dataset used for the urban and watercourse portions. In the last case, the

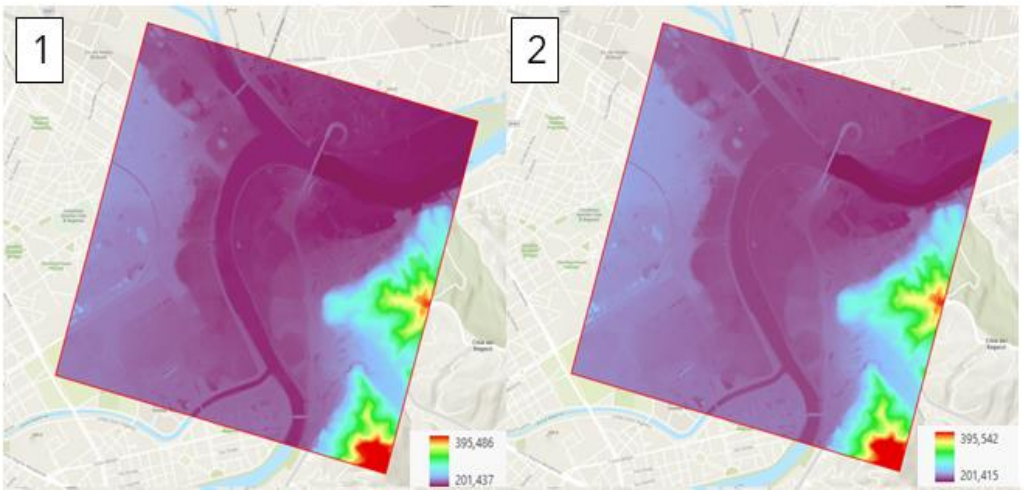


*Figure 5: $DTM_f$ (1) and $DTM_f$ (2) representation.*

elevation values display a lower elevation range compared to the other examples. This difference arises from missing data in the lower right corner of $DTM_f$ (4).

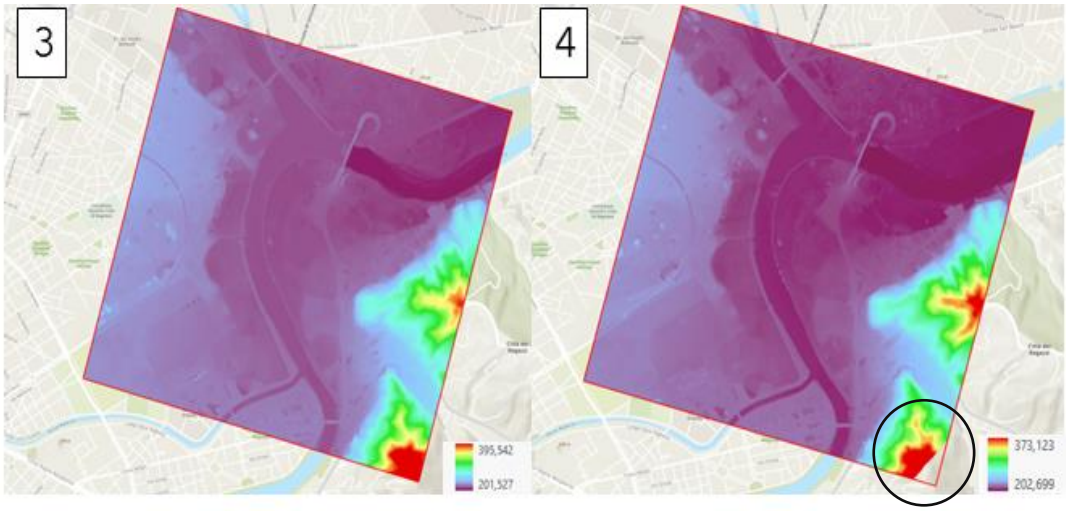


*Figure 6: $DTM_f$ (3) and $DTM_f$ (4) representation.*

## 2.4 Validation Process

After processing the data and generating the final DTMs, the next crucial step was to validate the results. To accomplish this, a set of high-precision elevation points within the Area of Interest (AOI) was collected from the Piedmont Regional Geoportal. Figure 7 illustrates the distribution of the 85 points used for the validation process.

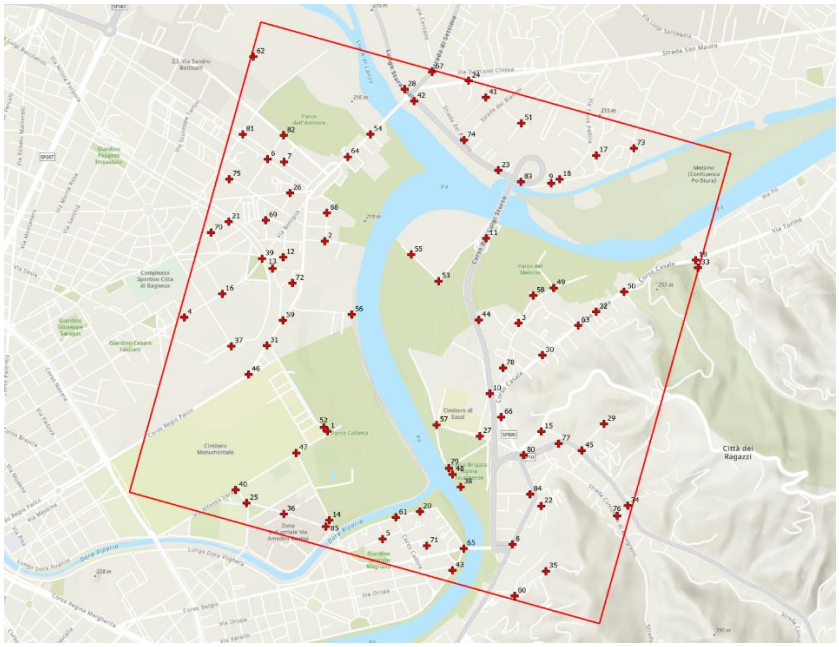

*Figure 7: Distribution of high precision elevation points.*

The validation procedure involves comparing the elevation data from these high-precision reference points with the corresponding points extracted from each of the final DTMs. This comparison allows the calculation of statistical parameters to assess the discrepancies between the datasets, enabling a comprehensive analysis of errors to evaluate the accuracy and reliability of the final outputs.

In order to assess the reliability of the LiDAR point clouds, a similar procedure was followed. At this stage, for each point of the reference dataset, the closest point from the cloud was manually assigned. Subsequently, the elevation values for the regional point and the corresponding ones extracted from the different DTMs were compared. Statistical parameters are then calculated based on the differences between these values. The results of the statistical analysis are presented in the following table:

| | **Difference in meters (m) between regional elevation points and $DTM_f$ *(i)* and original *LiDAR point cloud*** | | | | |
|---|---|---|---|---|---|
| | ***$DTM_f$ (1)*** | ***$DTM_f$ (2)*** | ***$DTM_f$ (3)*** | ***$DTM_f$ (4)*** | ***Original LiDAR point cloud*** |
| **Max** | -0.27 | -0.28 | -0.93 | 0.09 | 1.31 |
| **Min** | 0.99 | 1.00 | 1.00 | -1.21 | -0.30 |
| **Average** | 0.32 | 0.32 | 0.30 | -0.59 | 0.33 |
| **Median** | 0.34 | 0.33 | 0.34 | -0.55 | 0.37 |
| **Stand. Dev.** | 0.30 | 0.30 | 0.34 | 0.31 | 0.33 |
| **RMSE** | **0.44** | **0.44** | 0.46 | 0.66 | 0.46 |
| **MAD** | 0.25 | 0.25 | 0.27 | 0.26 | 0.27 |
| **NMAD** | 0.37 | 0.37 | 0.40 | 0.38 | 0.40 |

*Table 3: Statistical parameters for the difference between reference data (region elevation points) and data processed ($DTM_f$ or LiDAR point cloud)*

## 2.5 Considerations

The results presented in Table 3 demonstrate that the various combinations used to generate the final $DTM_f$ produced differing levels of accuracy. It is essential to acknowledge that several factors can contribute to errors and uncertainties, which subsequently influence the outcomes of the validation process.

Firstly, the LiDAR point cloud acquisitions conducted by the Ministry of the Environment and DTM produced by the Po Basin Authority, were performed using survey equipment that might be considerably different from those available today or in 2022 when the Polytechnic School of Turin conducted the acquisition. This discrepancy in technological advancements can lead to accuracy errors when comparing and combining data from these different sources against the reference data.

Systematic errors that occurred during the data acquisition process must also be considered as they can impact the accuracy of the released data. Moreover, the temporal epochs of the reference data should be taken into account. It is possible that

morphological variations in the investigated territory occurred between the acquisition dates of the reference data and the LiDAR data, which could explain variations in elevation values observed between the processed and reference datasets. Finally, the processing phases play a significant role in the results. Depending on the different combinations of parameters used in the procedures, the final DTMs can exhibit variable levels of accuracy.

To address potential sources of error that could lead to inaccuracies in the results, it was decided to prioritize datasets closely matching the reference data, particularly the first and second combinations. In terms of assessing dataset quality against accurate reference data, the Root Mean Square Error (RMSE) and Normalized Mean Absolute Deviation (NMAD) are widely recognized as robust indicators for evaluating height data[6]. Our analysis showed that the first two combinations of data produced the most reliable results, as they exhibited lower RMSE and NMAD values. Conversely, the last two combinations have been computed with higher statistical parameter values, suggesting they might be less representative of the territory. Furthermore, an examination of the statistics comparing the LiDAR point cloud to the Piedmont regional elevation points revealed significant agreement between the datasets. This finding further confirms the validity of the data used as input for DTM generation in the first and second combinations, strengthening their reliability and accuracy.

Finally, the $DTM_f(2)$ with a 1m/pixel resolution has been selected as it provides higher precision. Utilizing high-resolution DTMs, it is expected higher accuracy in the elevation data to simulate flood scenarios and higher accuracy in predicting water flow patterns during various flood conditions.

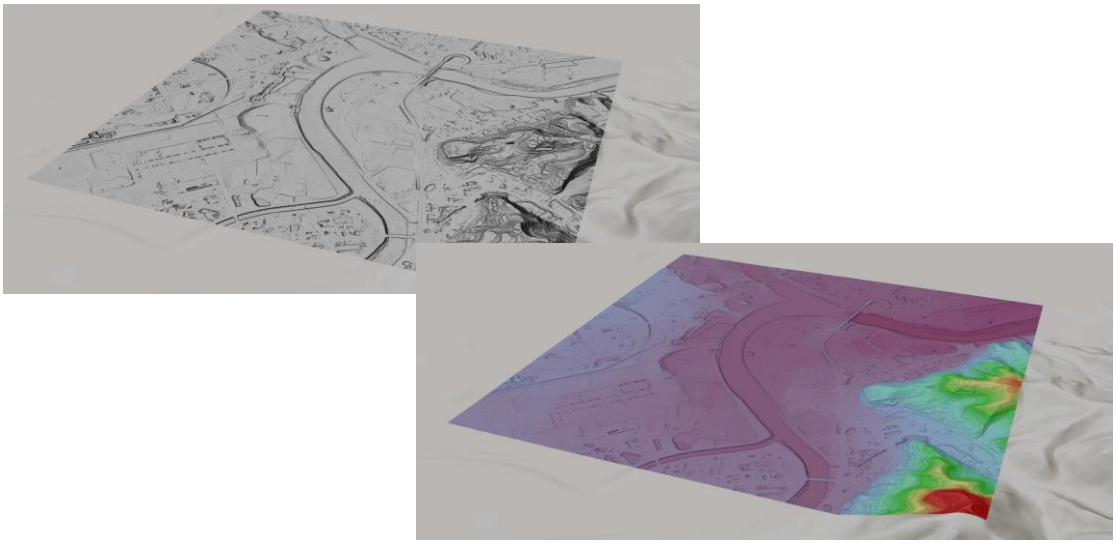

*Figure 8: 3D representation of the final DTM selected ($DTM_f(2)$)*

## 2.6 Digital Surface Model Generation

The high-density LiDAR dataset has been employed as well for extracting the Digital Surface Model (DSM) across the study area, offering a comprehensive three-dimensional representation of the Earth's surface[7]. This distinction from the Digital Terrain Model (DTM) is critical, especially within complex urban environments characterized by a dense presence of features such as trees, roads, bridges, and various infrastructure elements. In this context, the DSM assumes a crucial role since it contains precise elevation data essential for in-depth analyses of floodwater dynamics.

For the generation of the Digital Surface Model, ENVI LiDAR was utilized as well. The selected resolution for this model remained consistent at 1m/pixel, repeating the approach taken for DTM extraction. Similar to the challenges encountered during DTM generation, the DSM creation process faced difficulties in the river section. To mitigate the limited LiDAR data coverage over the river surface, the river portion of the final $DTM_f$ has been used. In this context, it's important to note that the primary focus was on the urban region of the area, where precise river elevation data wasn't a critical requirement for the study objectives.

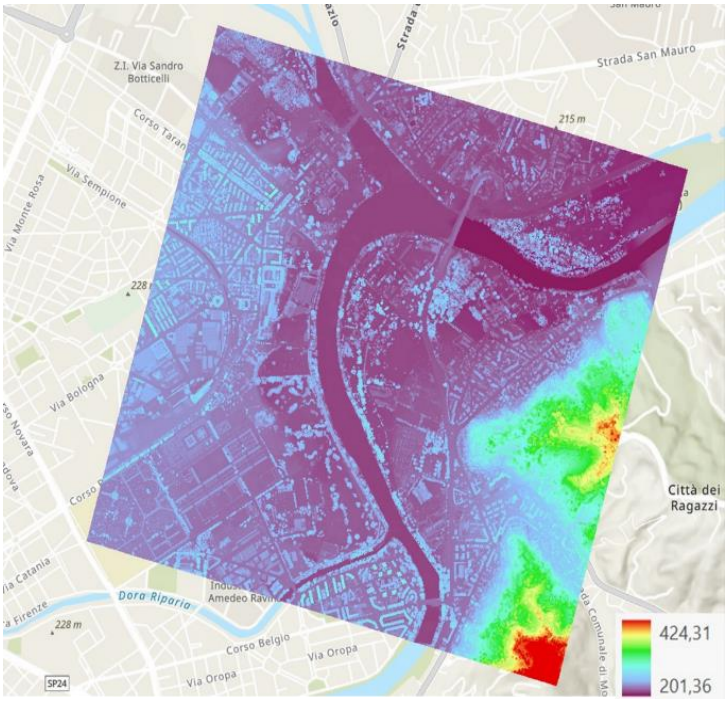


*Figure 9: Final DSM*

# Workflow Overview-DEM Generation

The data has been processed considering the steps described in workflow represented below.

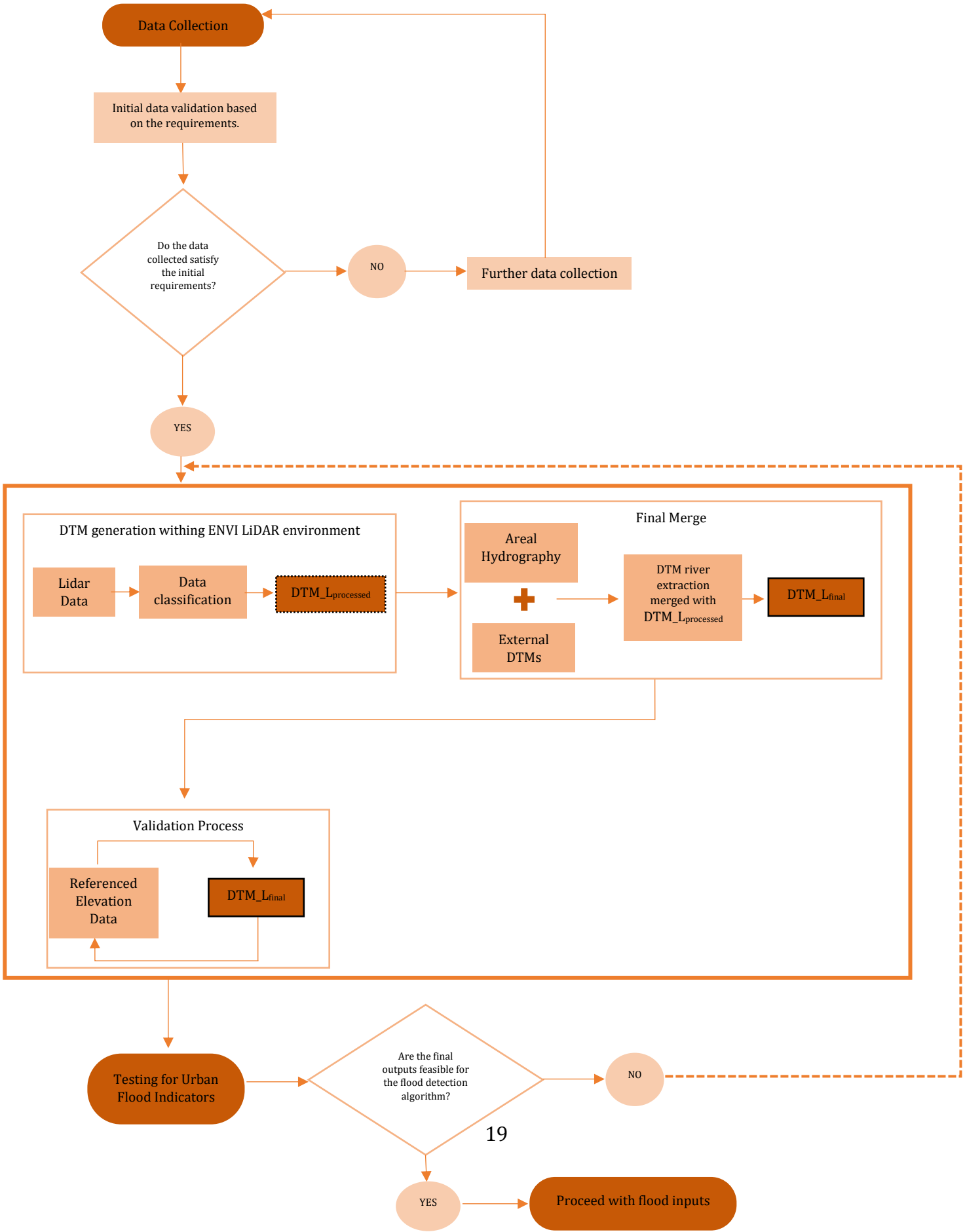

# 3. Features Extraction for Flood Modelling

In preparation for the flood assessment, the initial step involved the extraction of various surface features within the study area. This process plays a crucial role in calculating the runoff coefficient, as it directly depends on the types of features present on the surface. Key features extracted include buildings, trees, vegetated areas, streets, and other impermeable surfaces. In the following table there are presented the data sources of each feature class. For the buildings and trees features, even though they were directly extracted from ENVI Lidar, a refinement has been implemented using the Turin's Geoportal database, in order to correct any errors that could have been generated from the ENVI Lidar algorithm. Finally, the refinement has been also implemented using the orthophoto extracted from the LiDAR point cloud (Figure 10).

| Feature | Sources | |
|---|---|---|
| **Buildings** | Turin's Geoportal | LiDAR point cloud |
| **Roads** | Turin's Geoportal | / |
| **Trees** | / | LiDAR point cloud |

*Table 4: Feature's Source*

*Figure 10: Orthophoto of the AOI*

## 3.1 Buildings Extraction

In the context of urban flood assessment, the extraction of building footprints is crucial for understanding the interaction between floodwater and the urban environment. Initially, building extraction was conducted using ENVI LiDAR software. To ensure the accuracy of these results, a validation step was conducted using the feature dataset provided by the city of Turin (Geoportale Città di Torino) at a scale of 1:1000, along with the orthophoto produced from the LiDAR point cloud. This approach resulted in a highly reliable dataset for subsequent urban flood assessment steps. Elevation information was then assigned to the building footprints using ArcGIS's "Add Surface Information" tool, utilizing the DSM to determine roof elevation.

Figure 11 illustrates a comparison between the building footprints extracted with ENVI LiDAR (left) and those provided by the City of Turin (right).

*Figure 11:Building footprints ENVI LiDAR-Turin Geoportale dataset*

### 3.1.1 DSM Generation using breaklines

The extraction of building footprints has been an important aspect in the initial approach, where it was assumed that the DSM would be utilized for flood assessment. These footprints served as fundamental elements in defining breaklines within the terrain model. Breaklines are linear features that significantly influence the description of surface behavior when incorporated into a surface model. They can be assigned z-values along their length, providing essential information about abrupt changes in surface elevation[8].

To achieve this, the surface model has been generated using ArcGIS Pro instead of ENVI Lidar. ArcGIS Pro gives the possibility to choose between three types of breaklines:

- Soft breaklines
- Hard breaklines
- Faults.

For our study, hard breaklines option has been selected to represent abrupt changes in surface smoothness (Figure 12).

The resulting DSM exhibited some blurriness, particularly in the river section of the Area of Interest (AOI), similar to the challenges encountered during the DTM generation process. Despite maintaining a resolution consistent at 1m/pixel, similar to the DSM extracted from ENVI Lidar software, a more detailed representation has been observed in the DSM extracted with ENVI software. The two DSM results are presented below in a 3D view:

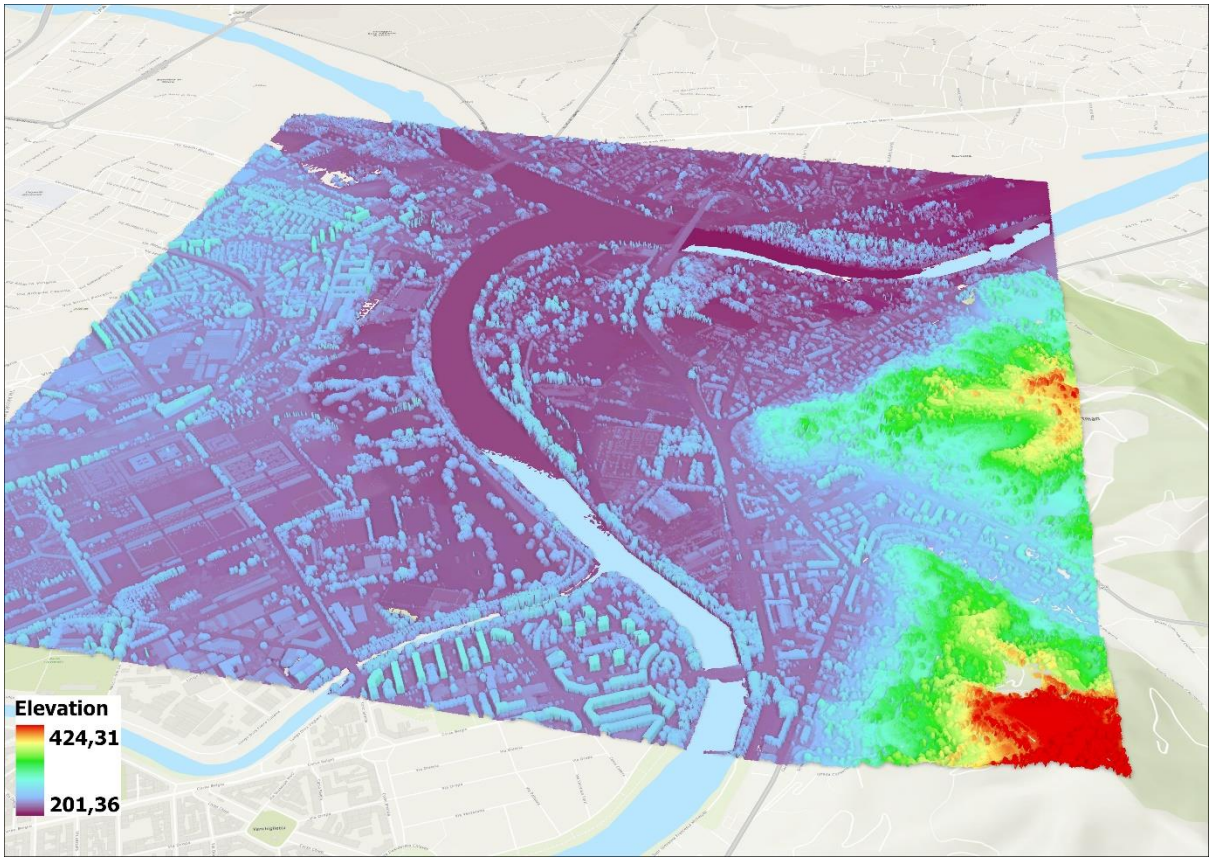


*Figure 12: DSM - ENVI Lidar*

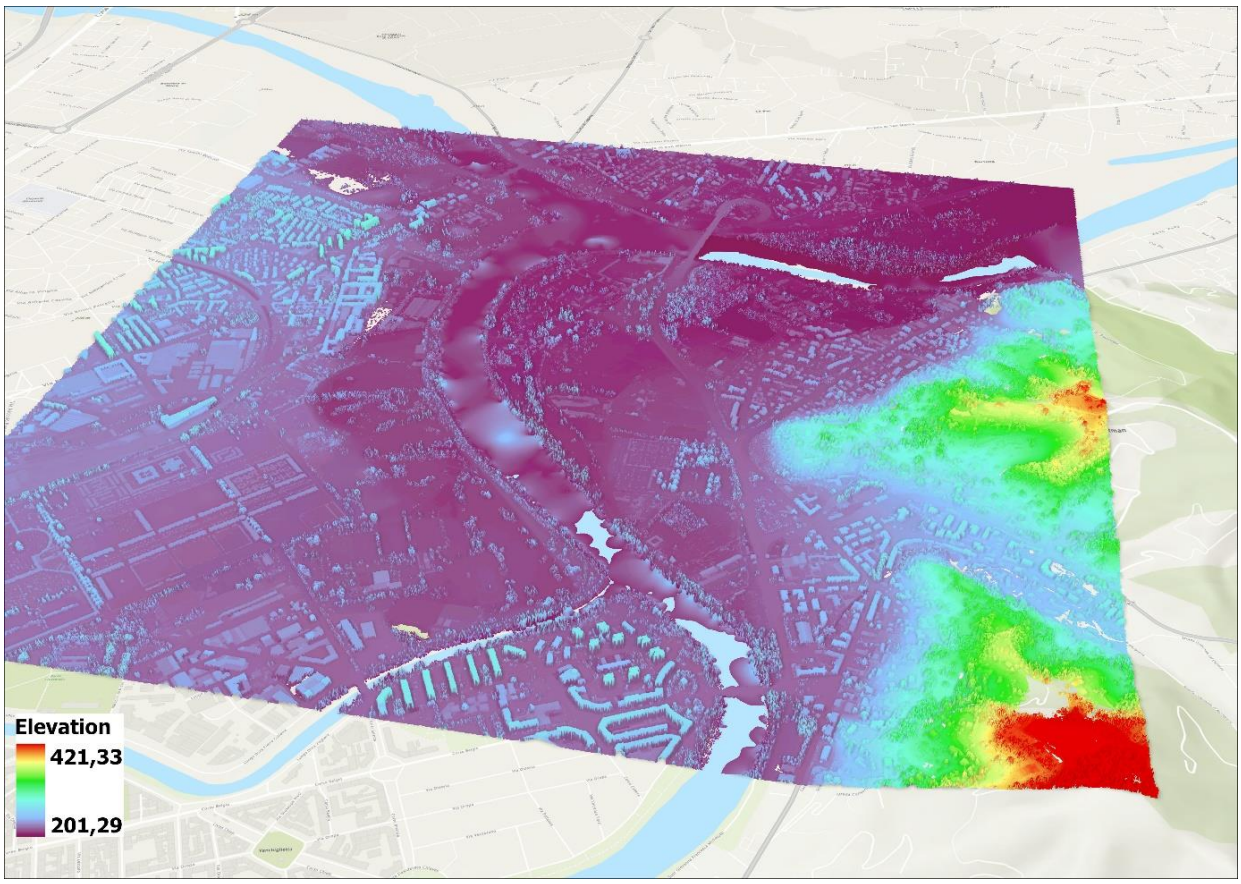


*Figure 13: DSM - ArcGIS Pro – breaklines*

# 3.2 Roads Extraction

The road extraction process represents a significant and time-consuming step in this thesis, involving multiple stages to achieve the desired accuracy. Road extraction was performed using two approaches. Firstly, the dataset from the geoportal of the city of Turin was utilized to obtain the areal features of each road within the Area of Interest (AOI), a dataset updated in 2009 (Figure 14). Subsequently, the centreline of each polygon was derived using QGIS software. It's worth noting that each polygon was associated with attributes, including street material (such as asphalt, gravel, or paved), road names, lengths, and condition assessments (ranging from good to degraded). The centreline generation was conducted to transform the roads from polygonal representations into linear features, while preserving the attributes. Moreover, after creating these centrelines a manual shape-fixing process was implemented to further enhance the accuracy of the road representations, ensuring that the road network was not only complete but also precisely aligned with the real-world geography. A final refinement of the lines has been done using the orthophoto of the area.

In the first approach regarding the inputs of the hydrological model, the slope of the roads has been estimated. For roads less than 500 meters in length, the calculation of the slope has been implemented using elevation data from the Digital Terrain Model (DTM). In detail the elevation value at the first and last point of each road has been used dividing by the total length of each segment.

$$Slope = \frac{DSM_{Elevation\_2} - DSM_{Elevation\_1}}{Total\ Length}$$

Roads longer than 500 meters were subdivided into smaller sections, following the same slope calculation. This approach provided slope variations in the range of 0 to 20 degrees, with the steepest slopes mainly found in the hilly parts of the city. In Figure 16 the legend for each slope category is presented.

It's important to note that, for the final hydrological modelling inputs, only the polygons representing the streets were utilized in order to simplify the study.

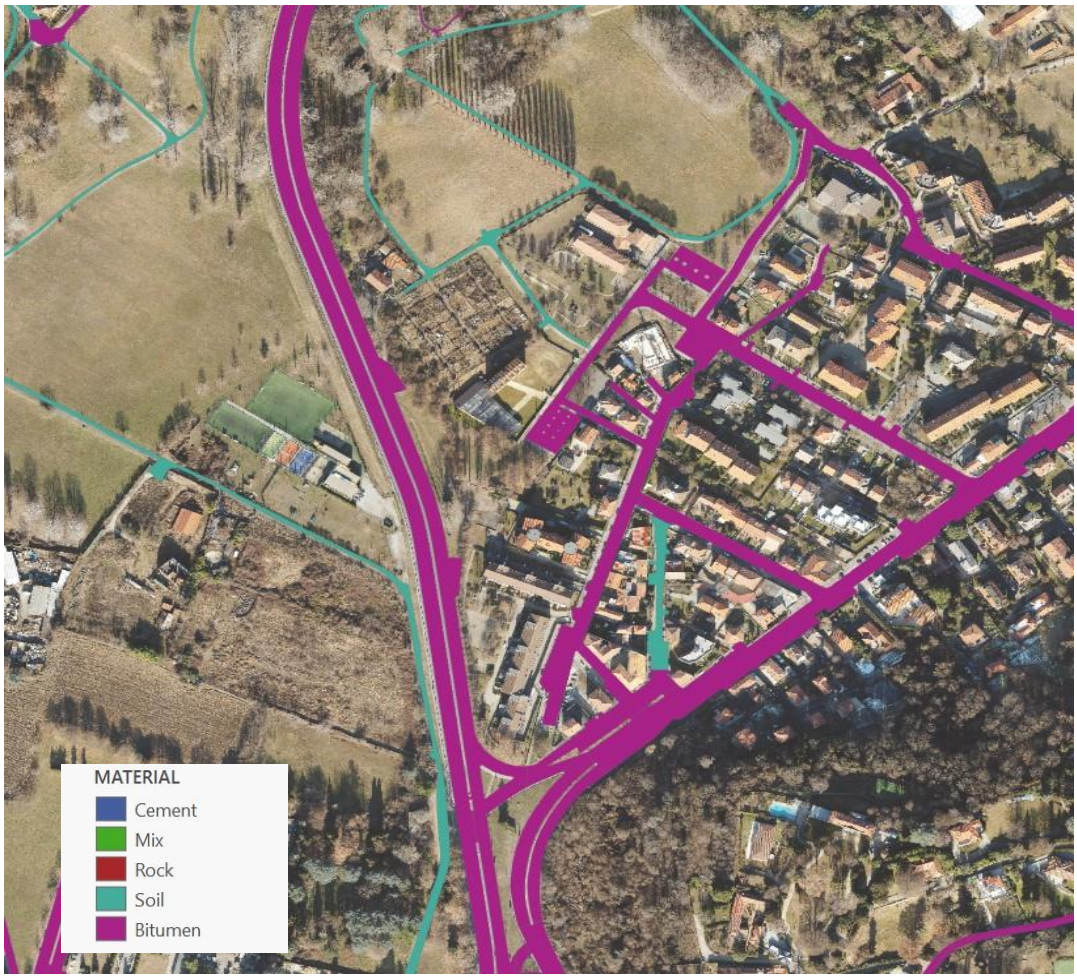


*Figure 14: Road Polygon Features*

*Figure 15: Road Centerline*


*Figure 16: Road slope*

# 3.3 Trees Extraction

Using Envi LiDAR, it is possible to extract trees from the LiDAR point cloud data. During this extraction process, the default parameters of the software have been maintained, which included a minimum height of 130 cm and a minimum radius of 200 cm. While the results of this extraction have generally been satisfactory, they have not been entirely accurate. Notably, in areas where trees exhibit large crowns (Figure 17), there has been a tendency to overestimate the presence of trees, resulting in an identification of more trees than are actually present. Consequently, manual refinement was required using the orthophoto.

In order to accurately incorporate the trees into the runoff coefficient calculation, the buffer tool within ArcGIS has been employed. This tool allowed to create a buffer zone around each tree point, effectively transforming them into spatial areas rather than points (Figure 18). By establishing a buffer with a radius of 5 meters around each tree, it was possible to consider the spatial extent of the tree canopy and its potential influence on runoff. This approach ensures that the runoff coefficient calculation takes into account not only the presence of individual trees but also their surrounding area, providing a more comprehensive assessment of their impact on the hydrological system.

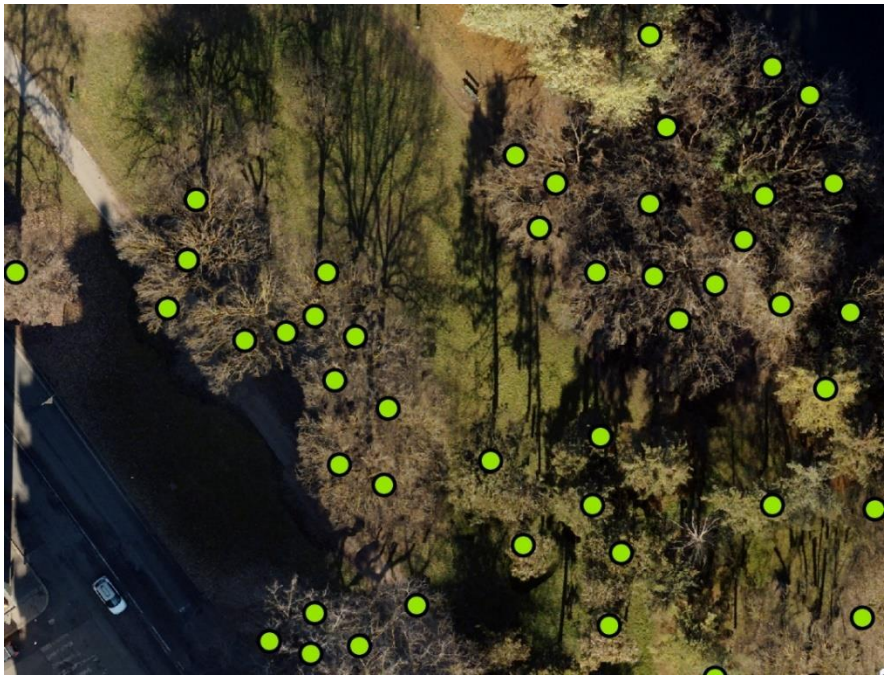

*Figure 15: Overestimation of trees*

*Figure 16: Tree Buffer Areas*

# 3.4 ENVI - Supervised Classification

While the initial data extracted from databases offered valuable insights, it became apparent that they were insufficient for precisely calculating the runoff coefficient, as numerous areas remained unclassified. In response to this limitation, supervised classification with ENVI was chosen. ENVI supervised classification is a method used to categorize pixels in an image into different classes based on user-defined training data. This process involves specifying training areas, also known as regions of interest (ROIs), and they must be defined before the launching of the classification. There have been considered 5 different classes:

1. Water surface
2. Trees
3. Sparse Vegetation
4. Buildings
5. Roads

These classes were then grouped into two overarching categories: permeable and impermeable surfaces.

The classification method used has been based on the Maximum Likelihood which means that each pixel is assigned to the class with the highest probability[9]. The result of the classification is presented in Figure 20.

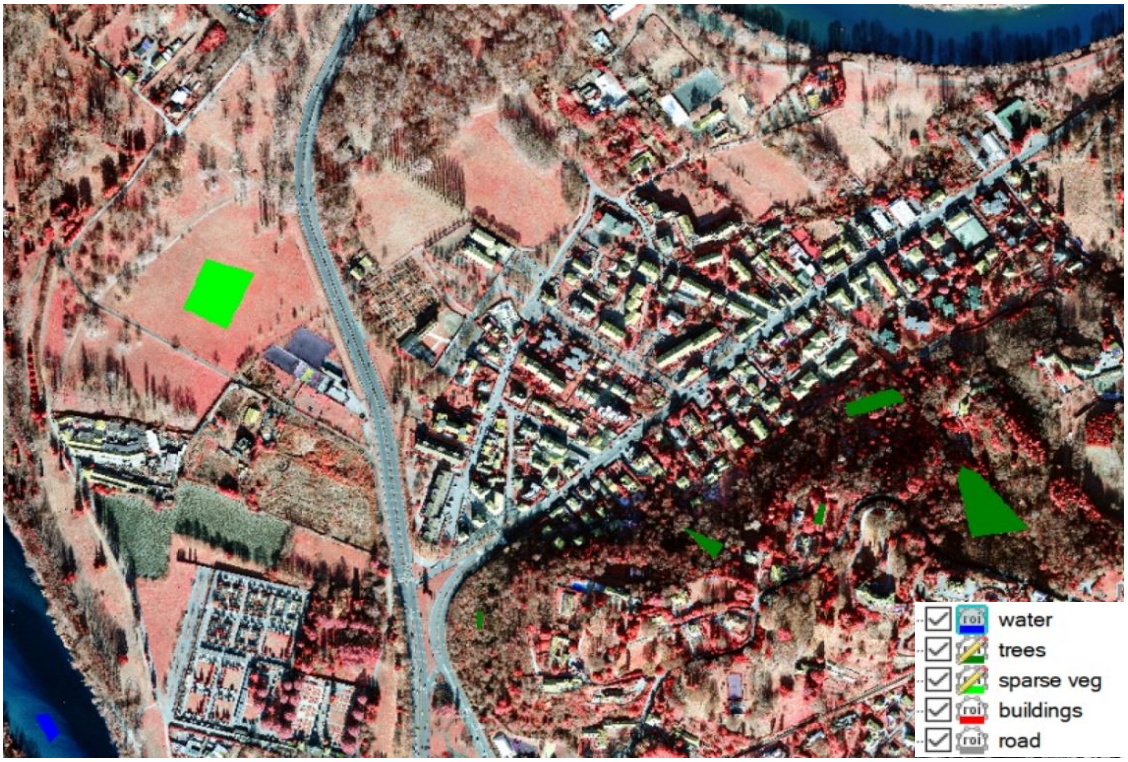


*Figure 18:ROIs Definition*

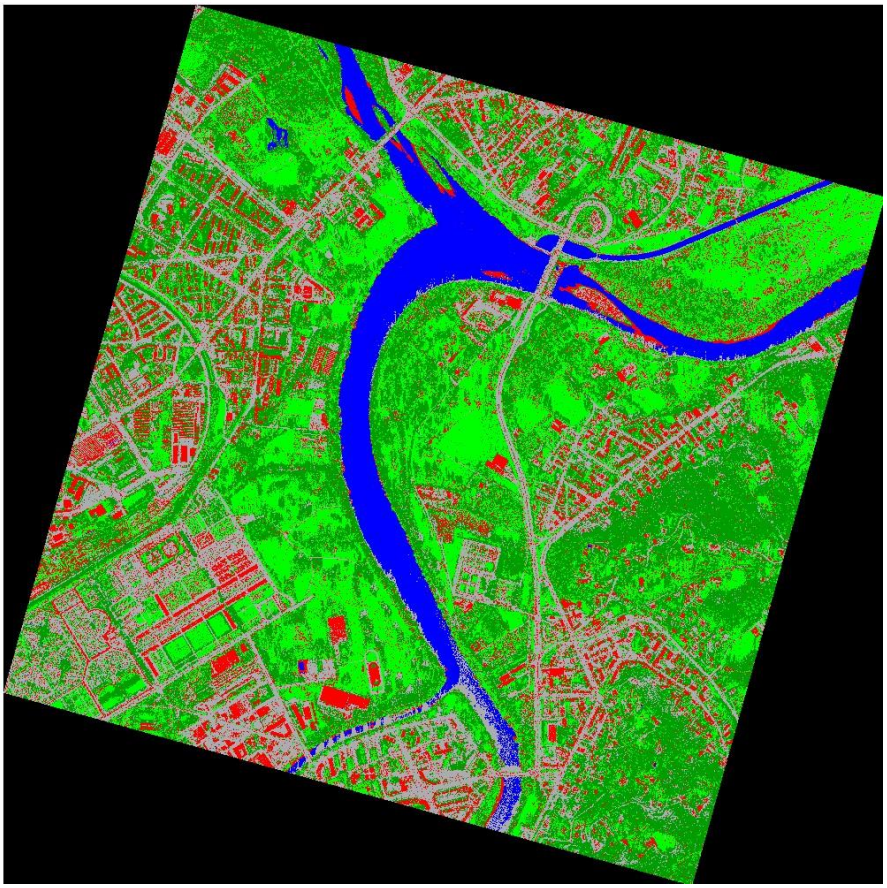

*Figure 17: Final Classification*

The final workflow in the feature extraction is presented below:

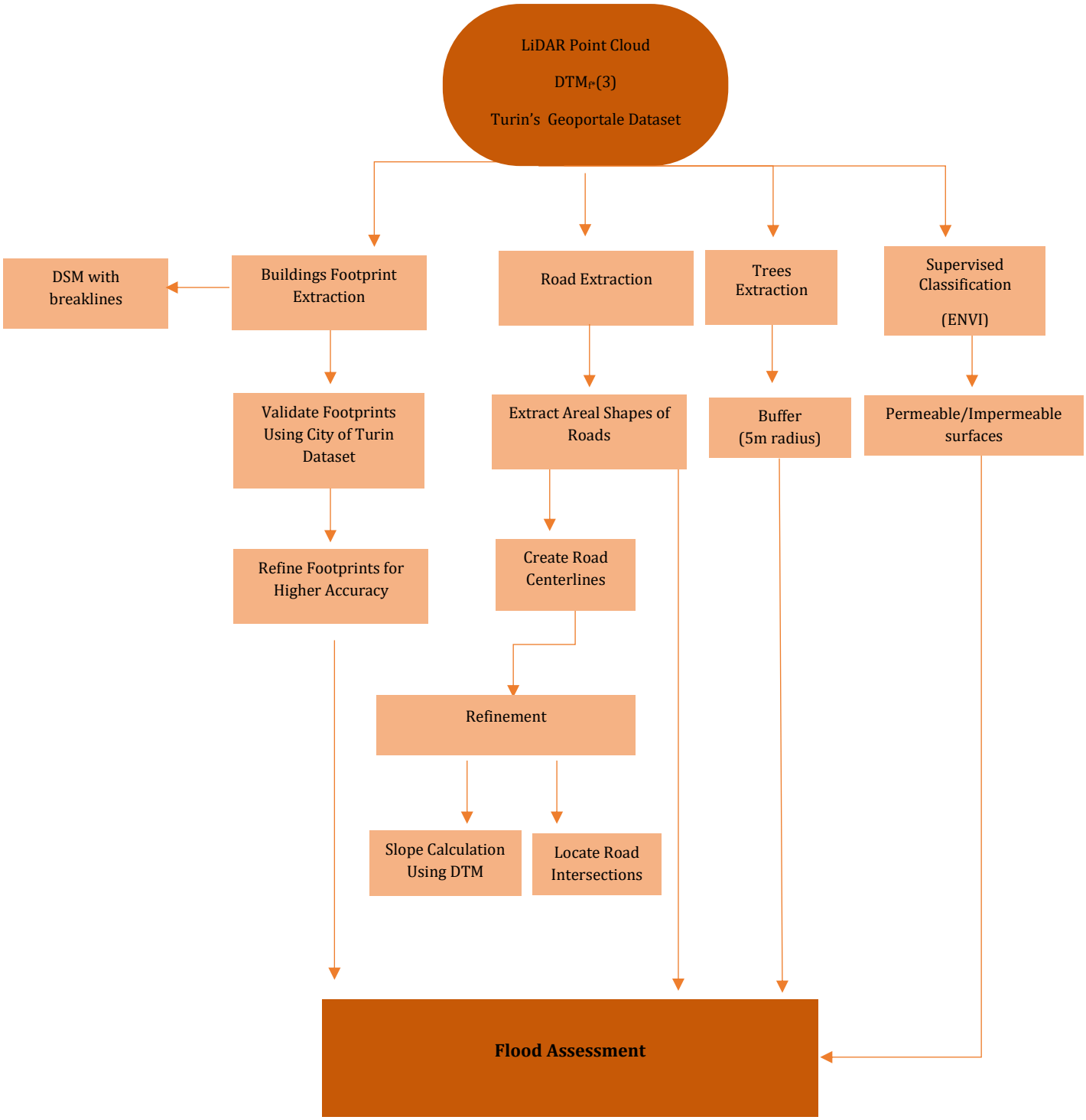

# 4. Flood Assessment

Flooding events pose a growing threat to urban areas. This phenomenon can be triggered by factors such as heavy rainfall (Pluvial Flooding), river overflow, and alterations in the climate patterns. It not only damages infrastructure but also puts lives at risk, making flood assessment crucial for effective mitigation strategies.

Pluvial flooding occurs when precipitation, typically absorbed by the ground or drained away, accumulates on impermeable surfaces. This type of flooding occurs when the intensity of rainfall surpasses both the capacity of stormwater drains and the ground's ability to absorb water. Pluvial flooding is often associated with short, intense storms lasting up to three hours, with rainfall rates exceeding 20-25 mm/hour. Additionally, it can occur after prolonged periods of lower intensity rainfall (10mm/hour), particularly in impermeable ground surfaces[10].

Due to these reasons, the implementation of GIS-based hydrological studies provide invaluable insights into how water flows across the territory, accumulates in low-lying areas, and interacts with drainage systems. By simulating and analysing these hydrological processes, it is possible to identify possible vulnerable areas, prone to flooding, and facilitate the development of effective mitigation strategies. Overall, the incorporation of hydrological studies within GIS systems plays a fundamental role in building resilient cities and safeguarding communities against the adverse impacts of flooding events.

## 4.1 Flood Assessment - Overview

The Flood Assessment section is a crucial component of this thesis, as it uses the previously obtained results into practical application. Following the classification of all features within the digital elevation model, the focus shifts to evaluating flooding dynamics across the area under study, considering various precipitation scenarios. Due to the lack of data across the entire study area, analysis has been concentrated solely on the southernmost region (Figure 21).

The assessment is concentrated around examining the response of street inlets to differing precipitation intensities and potential clogging scenarios. The operational condition of components within urban drainage systems, such as street inlets, has a crucial role in their hydraulic performance. Inlets serve as entry points for surface stormwater runoff into the underground drainage network. However, the accumulation of debris can lead to partial or full blockage of these inlets, significantly impacting their functionality. Various factors, such as maintenance practices, the inlet's location, seasonal variations (such as leaf fall rates in autumn), can influence the extent of

blockage in inlets. Due to these reasons, three street inlet blocking scenarios have been analysed:

- 0% clogging, where all street inlets are assumed to be active.
- 10% clogging, indicating that 90% of street inlets remain active.
- 50% clogging, where only 50% of street inlets are assumed to be active.

For the practical aspect of this study, ArcGIS Pro has been used as the primary tool, facilitating the workflow for locating street inlets and obtaining elevation data. Our focus was on utilizing the Digital Terrain Model (DTM) to capture key topographic features, crucial for understanding natural water flow dynamics during flood occurrences. Additionally, in the analysis of runoff coefficients, the extracted feature classes have been used to enhance the accuracy of the assessment.

To ensure the highest accuracy in the analysis, two distinct workflows were implemented. The initial four steps remained consistent in both cases, but the deviation emerged from the fifth step onward.

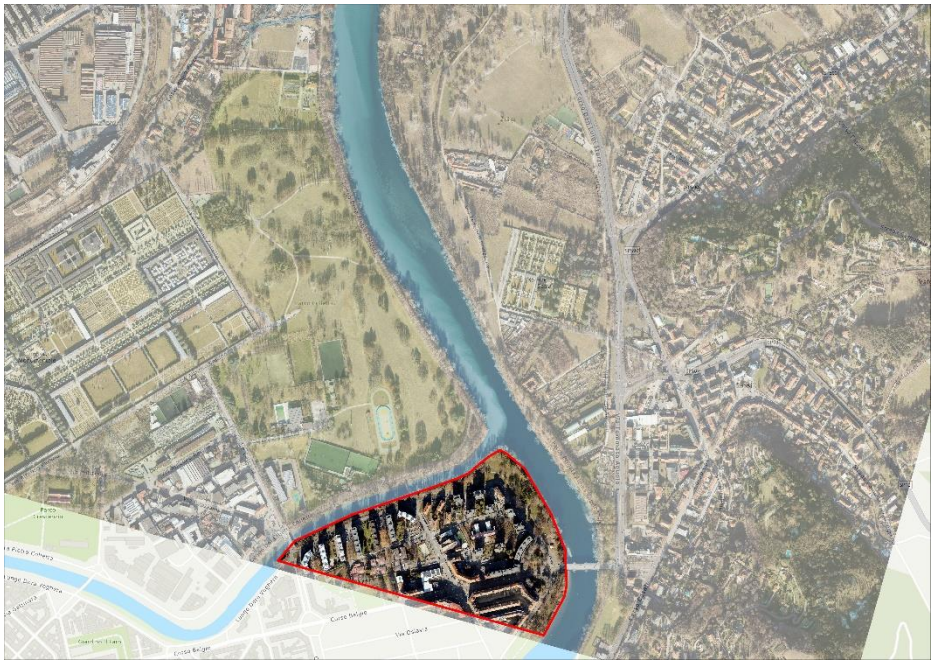

*Figure 19:AOI for flood assessment*

## 4.2 Hydrological Analysis - Methodology

At this stage of the study, two different approaches, Workflow 1 and Workflow 2, have been employed for sub catchment delineation. Initially, Workflow 1 involved a more complicated process that utilized street inlets as pour points and modifications to the initial DTM. However, discrepancies in the results of the surface runoff calculation shifted the analysis to the second Workflow where the toolbox ArcHydro has been used. Despite this adjustment, both methodologies will be outlined in the thesis, along with their corresponding results. The first Workflow is presented below:

**Workflow 1**

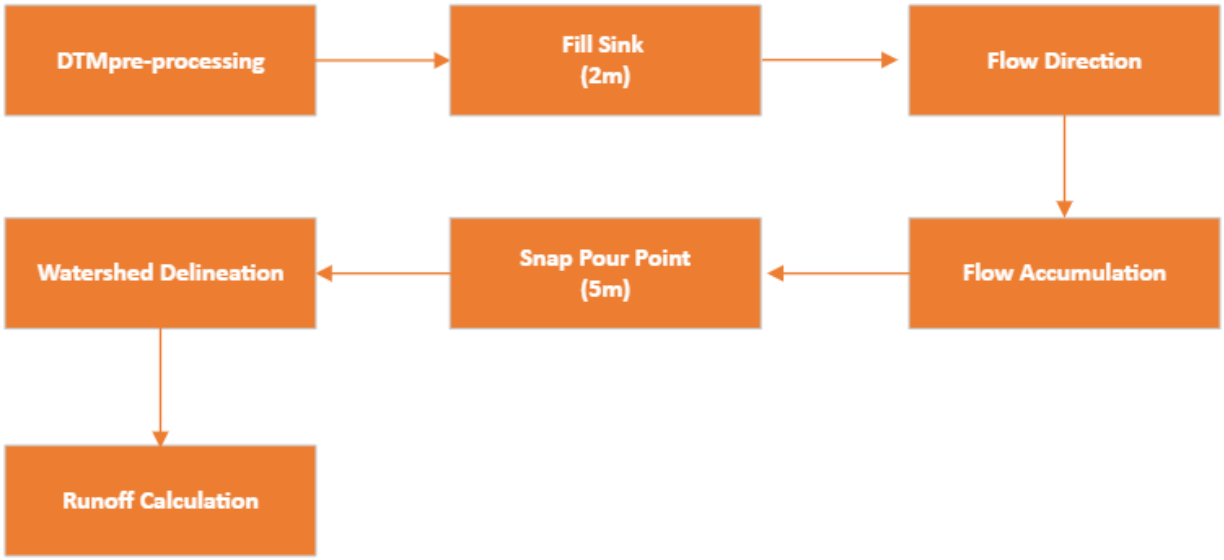


### 4.2.1 DTM pre-processing

In Workflow 1, the DTM underwent preprocessing by assigning a fictitious elevation of -10m to the street inlet points (Figure 22). This adjustment effectively transformed these points into real sinks that collect water and convey it to the conduits. In detail, the following procedure has been followed:

• Elevation value for street inlets feature class was assigned equal to -10 m

• Conversion of the point feature class to raster using the elevation as value to attribute to the resulted raster.

• Merging the initial raster DTM with the street inlet raster by overlaying the street inlet raster onto the DTM. The raster calculator tool was utilized for this purpose.

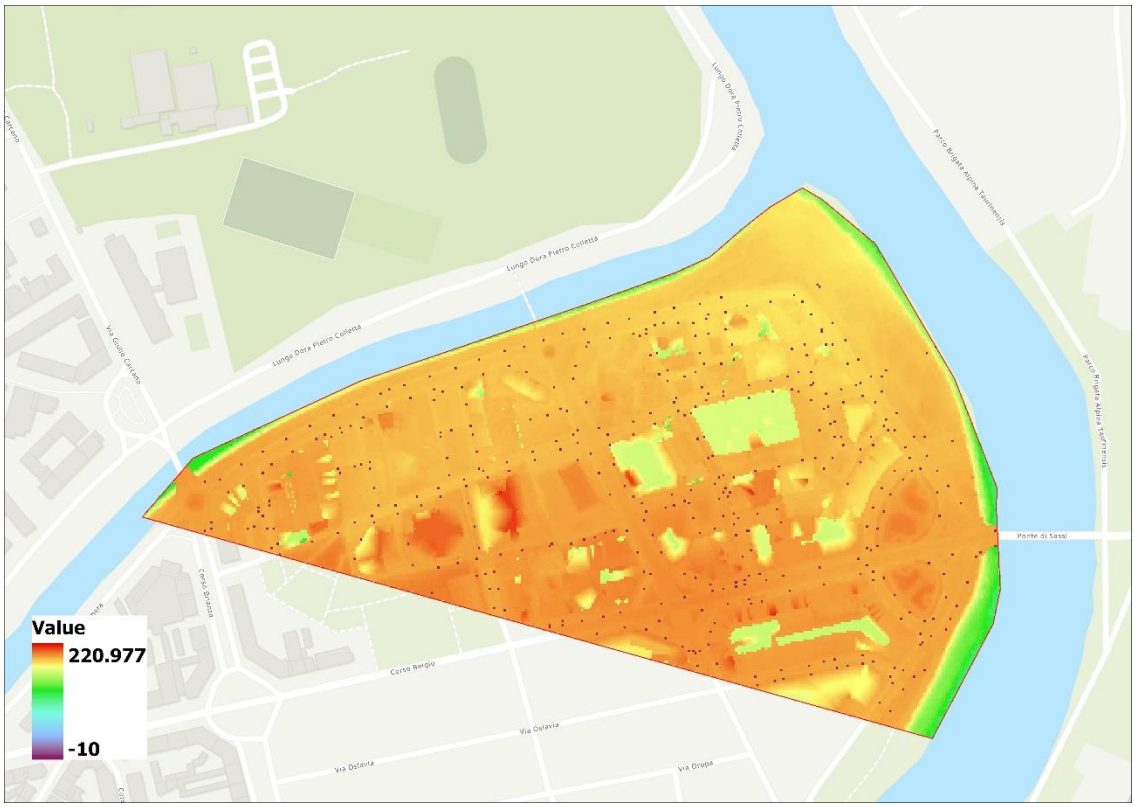


*Figure 20: Merged DTM*

## 4.2.2 Fill Sinks

A common issue encountered in digital elevation models (DEMs) is the presence of sinks and peaks generated from errors due to the resolution of the data or the rounding of elevations to the nearest integer value[12]. These errors can significantly impact hydrological analysis, particularly in tasks such as flow direction determination and watershed delineation. Sinks are essentially areas where all neighbouring cells have higher elevations, causing the flow algorithm to terminate prematurely if they are not addressed. To mitigate this issue, a tool is utilized to iteratively fill sinks within a specified z limit. This z-limit specifies the maximum allowable difference between the depth of a sink and the pour point, thereby determining which sinks will be filled and which will remain untouched[13]. In our case study z has been chosen equal to 2. As sinks are filled, it's important to note that new ones may be created at the boundaries of the filled areas, necessitating further iterations to ensure accurate modelling of the terrain.

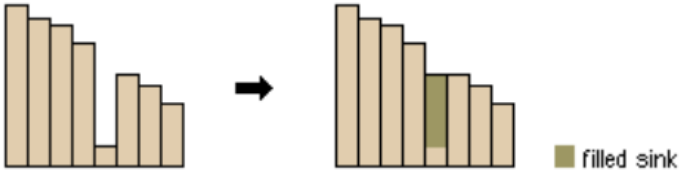


*Figure 21: Sink before and after Fill*

## 4.2.3 Flow Direction

The Flow Direction tool in ArcGIS Pro serves to produce a raster that illustrates the direction of water flow from each cell to its downslope neighbours. This functionality is crucial for hydrological modelling and analysis, providing information into the movement of water across terrain. The tool offers various methods for computing flow direction, including the D8, Multiple Flow Direction (MFD), and D-Infinity (DINF) methods[15]. For our specific case study, the D8 method has been employed, which calculates the flow direction from each cell to its steepest downslope neighbour. To understand the algorithm further, a brief explanation is followed.

The tool takes the Digital Terrain Model (DTM) as input, with each cell associated with a numerical value based on the slope of the terrain. After execution, the tool generates a raster grid indicating the flow direction for each cell using coded values, with each direction represented by a unique number (Figure 24). As there are eight potential directions for water flow, corresponding to the eight adjacent cells (according to the D8 flow model), the resulting raster presents these directional assignments. It is also worth noting, that "Force All Edge Cells to Flow Outward" option has been selected which means that all cells at the edge of the DTM surface will be forced to flow outwards and so no flowing back to the surface raster will be allowed.

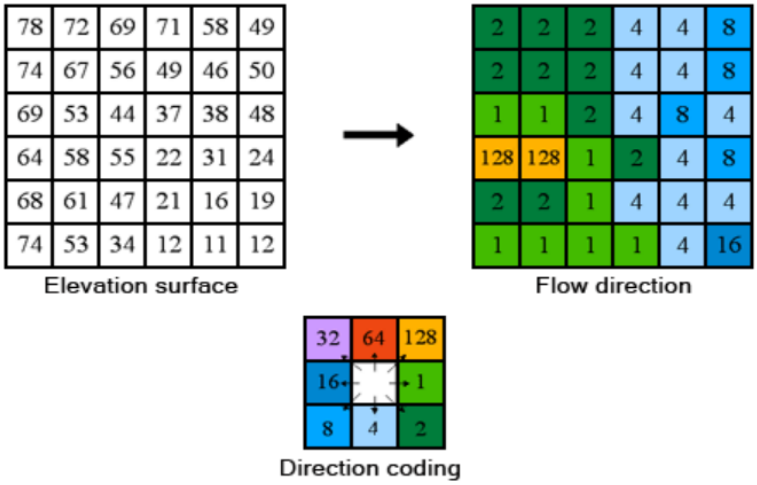


*Figure 22: Example of Flow Direction algorithm*

The directional coding of the flow is provided in the figure below:

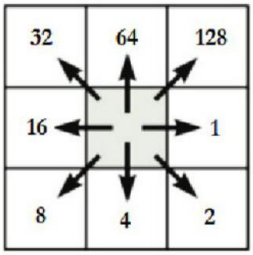


*Figure 23: Directional Flow Coding (Source: Adapted from Buarque et al. (2009))*

## 4.2.4 Flow Accumulation

Flow accumulation is fundamental in hydrological modelling, representing the accumulated flow as the sum of all cells flowing into each downslope cell in the output raster. Previously calculated flow direction raster is necessary in order to proceed with the flow accumulation. This process is crucial for identifying areas of concentrated flow, which can help in delineating stream channels, and for calculating indices like topographic wetness index (TWI)[16].

In the resulting flow accumulation raster, each cell value represents the number of raster cells contributing to that specific cell. A cell with a value of 0 indicates no contribution from other cells. Conversely, cells directly in the flow path for example are expected to show very high flow accumulation values. These cells, with their elevated flow accumulation values, demonstrate areas of concentrated flow and can help identify stream channels.

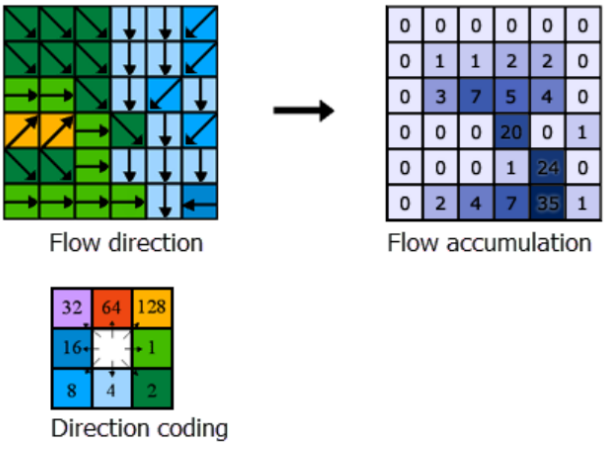


*Figure 24: Example of Flow Accumulation algorithm*

## 4.2.5 Snap Pour Point and Watershed Delineation

Street inlets have an essential role in urban drainage systems, serving as collection points for surface runoff directed into the stormwater network. In hydrological modelling, these street inlets are seen as pour points where water is expected to accumulate. The Snap Pour Point tool facilitates this process by snapping these points to the location with the highest flow accumulation within a specified distance[17]. In our case study, a distance of 5 meters was considered optimal as it ensured a continuity between the watersheds.
The final step involved delineating the watersheds in the area. A watershed refers to the upslope area that contributes flow to a common outlet in the form of concentrated drainage. It may be a part of a larger watershed and can also contain smaller watersheds known as sub catchments. The street inlet features were selected as outlet points or pour points for this purpose. During this process an important discrepancy has been observed as many street inlets were assigned to the same sub catchment, possibly due to the selection of the snap pour distance of 5 meters.

To better perform the repetitive process of iterating through the previous steps for all three scenarios and to find the optimal watershed representation, ModelBuilder in ArcGIS Pro was utilized. ModelBuilder serves as a visual programming language, allowing for the construction of complex workflows through a graphical interface. The models developed for this thesis, have been documented in Appendix A. Using ModelBuilder helped ensure consistency and efficiency in executing the required analyses across multiple scenarios [18].

## 4.2.6 Runoff Calculation

In this section of the thesis, the watershed delineation process was utilized to estimate the expected flow within each sub catchment. The following procedure has been made for both Workflows previously reported.

The digital terrain model (DTM) used for watershed creation did not account for buildings, which served as an initial simplification for this hydrological analysis. To calculate the runoff coefficient for each sub catchment, the percentage of each feature class within each area needed to be determined. This was achieved using the 'Tabulate Intersection' tool in ArcGIS Pro, which facilitated the calculation of percentages. The following feature classes were examined:

1. Tree Buffers (extracted from LiDAR point cloud)

2. Buildings (extracted from LiDAR point cloud)
3. Street Areas (obtained from Torino's Geoportal)
4. Permeable areas (areas not included in feature class 1 + sparse vegetation areas)
5. Impermeable areas (areas not included in feature classes 2 and 3)

It's crucial to highlight that all feature classes exhibited overlap, necessitating an initial clipping procedure before assessing the coverage percentage of each class. This process was repeated for all clogging scenarios. For the estimation of the runoff the rational formula has been used:

$$Q = \frac{C \times I \times A}{3.6} \times 1000 \quad (1)$$

Where:

Q: Run Off [L/s]

C: Run Off Coefficient

I: Rainfall Intensity [mm/h] (converted to mm/s)

A: Area of each sub catchment [$m^2$]

The Runoff has been calculated for 3 different Rainfall Intensity scenarios: 2mm/h, 20mm/h, 200mm/h.

The runoff coefficient (C) is a dimensionless coefficient relating the amount of runoff to the amount of precipitation received. It is a larger value for areas with low infiltration and high runoff (pavement, steep gradient), and lower for permeable, well vegetated areas (forest, flat land)[19]. For the Runoff Coefficient the following values have been considered based on the soil type:

| Soil Type | C |
|---|---|
| Trees | 0.3 |
| Buildings | 1 |
| Streets | 1 |
| Permeable (classification results) | 0.6 |
| Impermeable (classification results) | 1 |

*Table 5: Run Off Coefficients*

To compute the Runoff Coefficient, accounting for all land types, a weighted average method has been employed:

$$C = \frac{Trees_{\%} * 0.3 + Buildings\% * 1 + Streets\% * 1 + Permeable_{areas}\% * 0.6 + Impermeable_{areas}\% * 1}{100} \quad (2)$$

## 4.2.7 Workflow 1 Results

After the implementation of the 6 steps previously described the following results have been obtained. In the following figures the resulted watersheds for each clogging scenario are presented:


*Figure 25: Watersheds with 0% clogging*

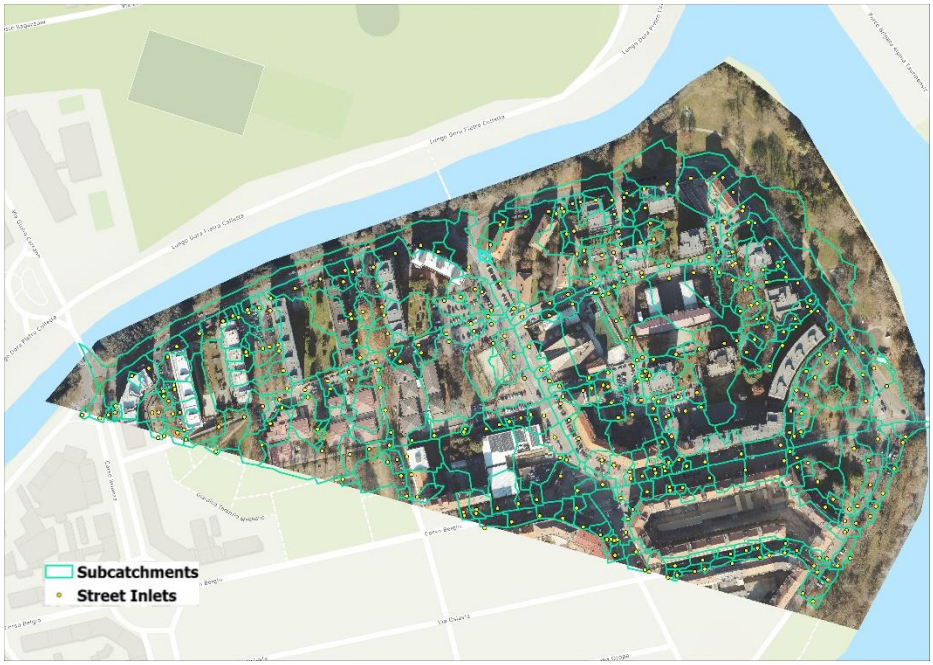


*Figure 26:Watersheds with 10% clogging*


*Figure 27: Watersheds with 50% clogging*

Using formula (1), the expected runoff associated to each street inlet has been computed, considering the three rainfall intensity scenarios (2mm/h, 20mm/h, 200mm/h). The number of street inlets analysed are 409 for the 0% clogging scenario, 368 for the 10% clogging scenario and 204 for the 50% clogging scenario. In the following tables a portion of the of the outcomes for each clogging scenario from the smallest to the highest runoff value:

| Street Inlets | Area | Street Class. | Vegetated Areas Class. | Buildings Class. | Trees | Streets | Buildings | Total | C | Q (2 mm/h) [L/s] | Q (20 mm/h) [m3/s] | Q (200 mm/h) [m3/s] |
|---|---|---|---|---|---|---|---|---|---|---|---|---|
| 218 | 26.18 | 0.22 | 5.48 | 4.52 | 89.78 | 0.00 | 0 | 100 | 0.35 | 0.001 | 0.01 | 0.14 |
| 415 | 38.36 | 0.32 | 22.34 | 1.43 | 65.33 | 10.58 | 0 | 100 | 0.45 | 0.003 | 0.03 | 0.27 |
| 419 | 20.00 | 0.00 | 0.00 | 0.00 | 0.00 | 100.00 | 0 | 100 | 1.00 | 0.003 | 0.03 | 0.31 |
| 204 | 43.93 | 0.35 | 5.41 | 16.51 | 71.08 | 6.65 | 0 | 100 | 0.48 | 0.003 | 0.03 | 0.33 |
| 434 | 69.16 | 0.13 | 2.99 | 0.01 | 96.88 | 0.00 | 0 | 100 | 0.31 | 0.003 | 0.03 | 0.33 |
| 238 | 22.20 | 2.44 | 1.74 | 41.31 | 0.00 | 54.51 | 0 | 100 | 0.99 | 0.003 | 0.03 | 0.34 |
| ... | ... | ... | ... | ... | ... | ... | ... | ... | ... | ... | ... | ... |
| 130 | 2961.20 | 1.57 | 15.26 | 17.26 | 13.01 | 4.62 | 48.27 | 100 | 0.85 | 0.387 | 3.87 | 38.71 |
| 309 | 3779.46 | 4.59 | 18.95 | 14.30 | 30.72 | 3.67 | 27.77 | 100 | 0.71 | 0.413 | 4.13 | 41.31 |
| 350 | 3278.47 | 5.37 | 23.18 | 21.35 | 11.96 | 5.26 | 32.88 | 100 | 0.82 | 0.416 | 4.16 | 41.65 |
| 240 | 2893.54 | 19.90 | 3.71 | 31.72 | 2.88 | 8.57 | 33.36 | 100 | 0.97 | 0.431 | 4.31 | 43.09 |
| 254 | 5091.72 | 2.53 | 28.31 | 23.16 | 9.13 | 1.13 | 35.74 | 100 | 0.82 | 0.646 | 6.46 | 64.60 |
| 406 | 9006.867 | 8.215418 | 12.82486 | 32.97875 | 0 | 3.224964 | 42.81695 | 100 | 0.95 | 1.318 | 13.18 | 131.77 |

*Table 6: Runoff - 0%*

| Street Inlets | Area | Street Class. | Vegetated Areas Class. | Buildings Class. | Trees | Streets | Buildings | Total | C | Q (2 mm/h) [L/s] | Q (20 mm/h) [m3/s] | Q (200 mm/h) [m3/s] |
|---|---|---|---|---|---|---|---|---|---|---|---|---|
| 261 | 2.74 | 98.85 | 1.15 | 0.00 | 0.00 | 0.00 | 0.00 | 100 | 0.995 | 0.0004 | 0.004 | 0.042 |
| 237 | 15.31 | 2.08 | 10.50 | 1.36 | 86.07 | 0.00 | 0.00 | 100 | 0.356 | 0.0008 | 0.008 | 0.084 |
| 250 | 24.23 | 0.01 | 1.66 | 0.00 | 98.33 | 0.00 | 0.00 | 100 | 0.305 | 0.0011 | 0.011 | 0.114 |
| 217 | 26.18 | 4.52 | 5.48 | 0.22 | 89.78 | 0.00 | 0.00 | 100 | 0.350 | 0.0014 | 0.014 | 0.141 |
| 397 | 24.69 | 0.05 | 26.36 | 1.91 | 71.67 | 0.00 | 0.00 | 100 | 0.393 | 0.0015 | 0.015 | 0.150 |
| 109 | 29.46 | 10.40 | 8.91 | 7.06 | 73.62 | 0.00 | 0.00 | 100 | 0.449 | 0.0020 | 0.020 | 0.204 |
| ... | ... | ... | ... | ... | ... | ... | ... | ... | ... | ... | ... | ... |
| 308 | 3810.32 | 14.34 | 18.85 | 4.70 | 30.45 | 3.62 | 28.04 | 100 | 0.711 | 0.4177 | 4.177 | 41.766 |
| 349 | 3304.86 | 21.16 | 23.00 | 5.36 | 11.86 | 6.01 | 32.61 | 100 | 0.825 | 0.4203 | 4.203 | 42.034 |
| 238 | 3086.47 | 29.73 | 3.43 | 18.65 | 2.16 | 14.90 | 31.14 | 100 | 0.971 | 0.4620 | 4.620 | 46.203 |
| 354 | 4464.64 | 7.05 | 3.75 | 0.96 | 8.04 | 79.57 | 0.64 | 100 | 0.929 | 0.6394 | 6.394 | 63.943 |
| 253 | 5059.61 | 23.27 | 28.46 | 2.54 | 8.68 | 1.08 | 35.96 | 100 | 0.825 | 0.6435 | 6.435 | 64.352 |
| 405 | 8896.15 | 33.44 | 12.98 | 8.34 | 0.00 | 2.10 | 43.15 | 100 | 0.948 | 1.3002 | 13.002 | 130.017 |

*Table 7: Runoff - 10%*

| Street Inlets | Area | Street Class. | Vegetated Areas Class. | Buildings Class. | Trees | Streets | Buildings | Total | C | Q (2 mm/h) [L/s] | Q (20 mm/h) [m3/s] | Q (200 mm/h) [m3/s] |
|---|---|---|---|---|---|---|---|---|---|---|---|---|
| 240 | 24.05 | 2.60 | 72.84 | 7.04 | 0.00 | 1.86 | 15.67 | 100 | 0.48 | 0.002 | 0.018 | 0.179 |
| 237 | 28.00 | 1.90 | 70.12 | 9.33 | 0.00 | 10.91 | 7.73 | 100 | 0.47 | 0.002 | 0.020 | 0.201 |
| 133 | 15.15 | 1.69 | 0.00 | 0.00 | 0.00 | 0.21 | 98.10 | 100 | 1.00 | 0.002 | 0.023 | 0.233 |
| 236 | 34.54 | 3.92 | 68.58 | 0.00 | 0.00 | 19.95 | 7.56 | 100 | 0.44 | 0.002 | 0.023 | 0.234 |
| 421 | 30.08 | 0.44 | 14.40 | 0.00 | 0.00 | 85.16 | 0.01 | 100 | 0.56 | 0.003 | 0.026 | 0.259 |
| 434 | 19.22 | 0.00 | 0.00 | 100.00 | 0.00 | 0.00 | 0.00 | 100 | 1.00 | 0.003 | 0.030 | 0.296 |
| ... | ... | ... | ... | ... | ... | ... | ... | ... | ... | ... | ... | ... |
| 308 | 4435.48 | 4.61 | 27.31 | 8.64 | 24.66 | 17.53 | 17.24 | 100 | 0.74 | 0.505 | 5.053 | 50.533 |
| 295 | 4168.79 | 4.29 | 8.68 | 9.35 | 18.36 | 33.78 | 25.54 | 100 | 0.80 | 0.517 | 5.167 | 51.672 |
| 329 | 4227.39 | 6.35 | 5.80 | 7.82 | 38.91 | 23.23 | 17.89 | 100 | 0.87 | 0.564 | 5.644 | 56.439 |
| 197 | 4487.02 | 5.93 | 15.14 | 0.01 | 29.33 | 13.59 | 36.01 | 100 | 0.84 | 0.581 | 5.811 | 58.107 |
| 337 | 5361.70 | 4.25 | 15.51 | 0.00 | 24.42 | 41.52 | 14.30 | 100 | 0.73 | 0.599 | 5.993 | 59.928 |
| 227 | 12047.30 | 2.90 | 12.04 | 11.59 | 25.55 | 27.14 | 20.79 | 100 | 0.81 | 1.499 | 14.988 | 149.883 |

*Table 8: Runoff - 50%*

The figure below illustrates the mean runoff value across the three clogging scenarios. Clearly, as the number of obstructed street inlets rises, there is a corresponding increase in the mean runoff value.

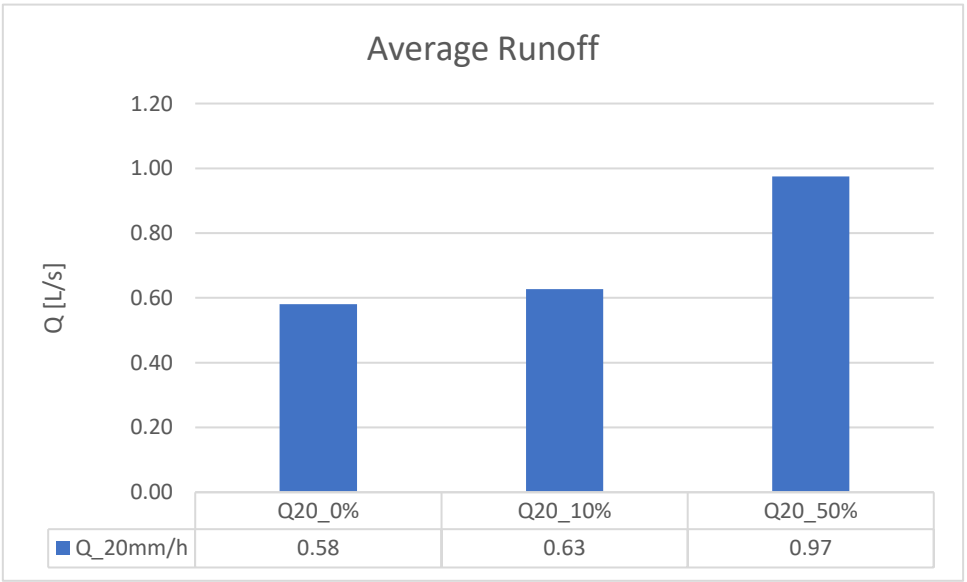


*Figure 28: Mean Runoff - Intermediate Rainfall Intesity*

The decision to alter the approach in watershed delineation derives from observations made during this initial method. It was noticed that numerous street inlets were grouped under the same sub catchments, suggesting potential inaccuracies in the runoff calculations. Furthermore, by analysing the runoff patterns when clogging the street inlets, a discrepancy was observed, red box area (Figure 31): for certain inlets, the runoff under the 0% scenario was unexpectedly higher compared to when other inlets were clogged. In real-world scenarios, it is expected that open street inlets would receive either the same or a higher volume of water. Hence, there was a need to investigate the number of street inlets exhibiting this inconsistency.

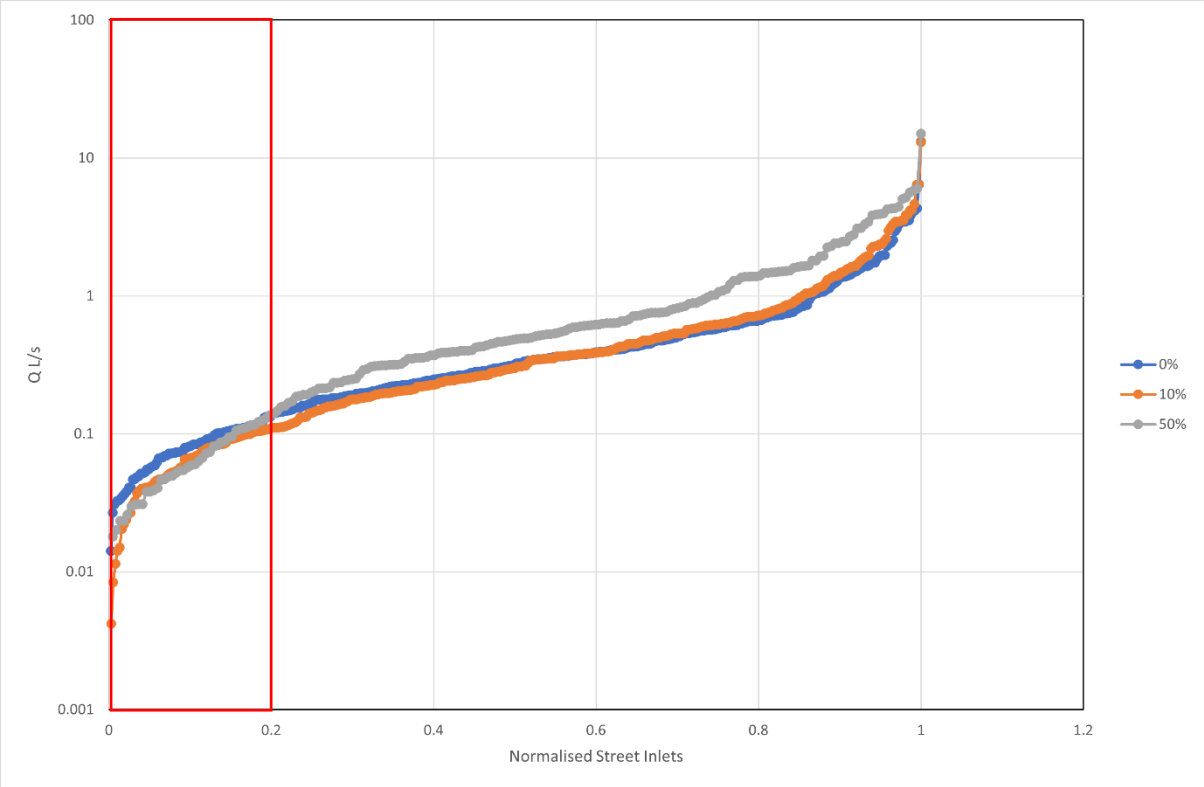


*Figure 29: Discrepancy in the Volume of Water Intake of Certain Street Inlets*

In order to better understand the observed difference, a comparative analysis was conducted between the 0% and 50% clogging scenarios using a scatter plot. This plot compares the runoff values (Q) of street inlets common to both scenarios, with the y-axis representing runoff values for the 50% clogging scenario and the x-axis representing values for the 0% clogging scenario.

The "bicept" line serves as a reference, indicating where the runoff values for the 0% and 50% clogging scenarios are equal. Points below this line represent street inlets where the runoff values are lower in the 50% clogging scenario compared to the 0% clogging scenario. This analysis helps identify street inlets where the expected runoff is lower when 50% of the inlets are clogged compared to when none are clogged and quantify this discrepancy (Figure 32).

The result of this analysis demonstrated that almost 36% of the street inlets present in the 50% scenario a lower discharge value in comparison to the 0% scenario. This result has been the reason of shifting to the second workflow.

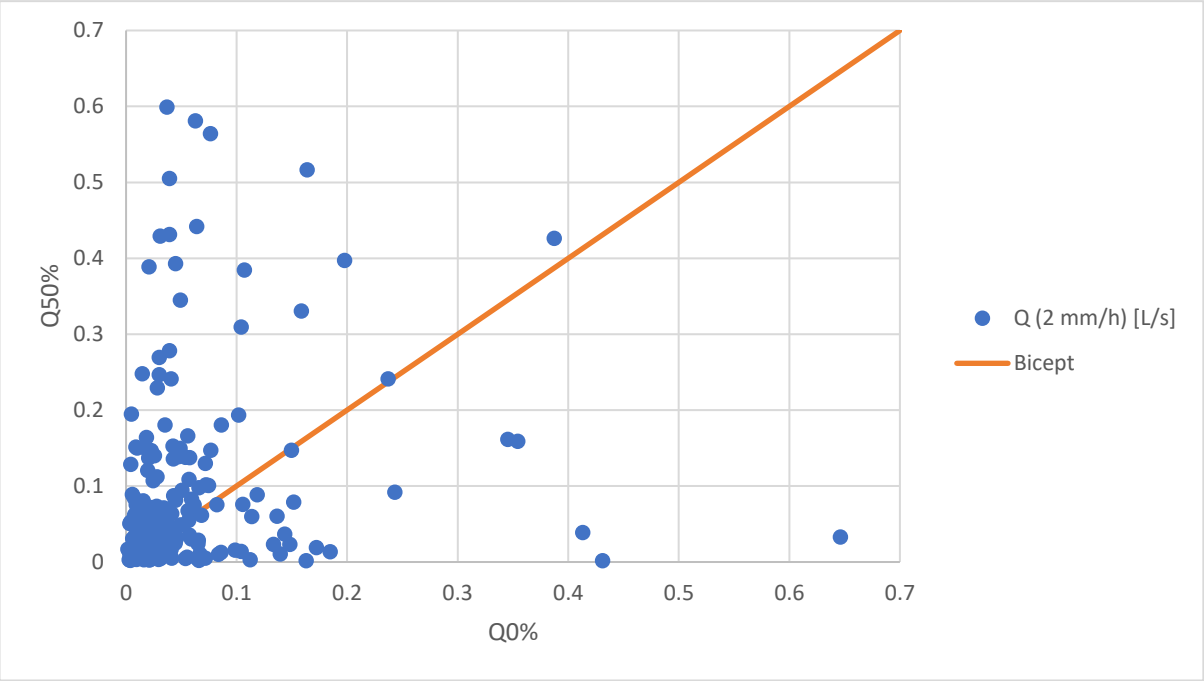


*Figure 32: Scatter Plot between the common street inlets*

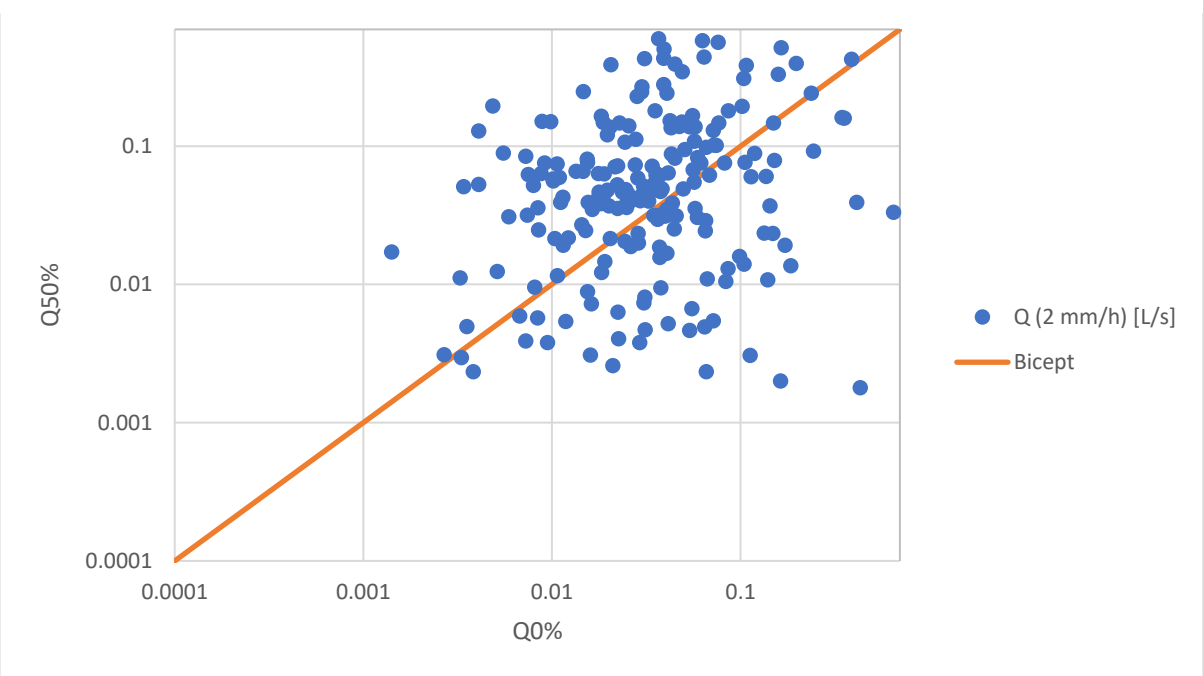


*Figure 33: Scatter Plot – Discrepancy Quantification between scenarios 0% and 50% - Log*

## 4.3 Hydrological Analysis – Modified Workflow

For the second workflow, a different approach was adopted to delineate the watersheds. In this case, the ArcHydro tool was utilized. ArcHydro is a robust tool specifically designed for hydrological modelling within the ArcGIS Pro environment. It offers versatility in various applications, including watershed delineation, stormwater management, and floodplain mapping. With ArcHydro, users can extract hydrological information from digital elevation models, derive runoff characteristics, and generate depressionless DEMs through processes like Fill Sinks[20].

The initial steps are those of the first workflow, including "Fill Sinks," "Flow Direction," and "Flow Accumulation." However, unlike the first workflow, the initial DTM used as an input remained unprocessed with no fictitious elevations assigned. This distinction marks a notable difference between the two workflows in terms of processing and data results. The workflow followed is presented below:

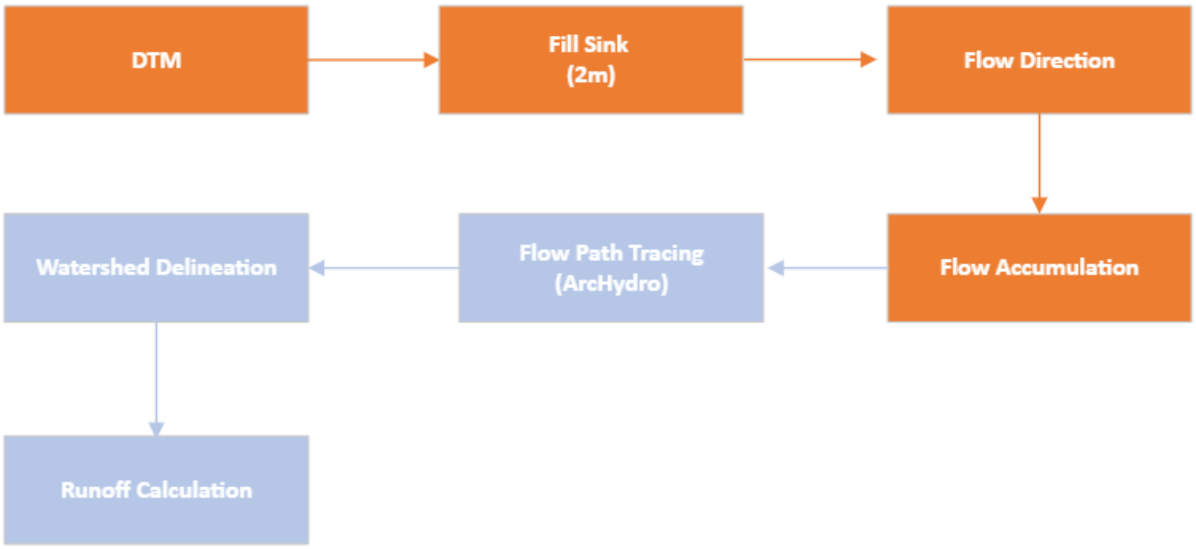


### 4.3.1 Flow Path Tracing

A significant aspect of this process was the utilization of the "Flow Path Tracing" tool, which facilitated the delineation of watersheds for each street inlet. This tool enabled the tracing of flow paths from specific points, such as street inlets, across the terrain. By

following these flow paths, the tool identified and delineated the contributing area or watershed for each inlet.

The workflow was repeated for 0% clogging, 10% clogging, and 50% clogging scenarios to comprehensively assess their impact on watershed delineation and flow patterns. In order to reduce the time processing of these processes Model Builder has been used also in this case.

## 4.3.2 Workflow 2 Results

After the implementation of the 'Flow Path Tracing' step previously described the following results have been obtained. In the following figures the resulted watersheds for each clogging scenario are presented:


*Figure 304:Watersheds_2 with 0% clogging*


*Figure 35:Watersheds_2 with 10% clogging*


*Figure 36:Watersheds_2 with 50% clogging*

The same procedure as in Workflow 1 has been followed for the calculation of the Runoff. The following tables illustrate the results of this calculation for all three scenarios:

| Street Inle | Shape_Len | Area | Trees | Buildings | Streets | Build Class. | Streets Class. | Vegetated Areas Class. | Total | C | Q (2 mm/h) [L/s] | Q (20 mm/h) [L/s] | Q (200 mm/h) [L/s] |
|---|---|---|---|---|---|---|---|---|---|---|---|---|---|
| 204 | 7.55 | 2.74 | 100.00 | 0.00 | 0.00 | 0.00 | 0.00 | 0.00 | 100 | 0.3 | 0.0001 | 0.0013 | 0.0127 |
| 89 | 7.55 | 2.74 | 81.47 | 0.00 | 18.53 | 0.00 | 0.00 | 0.00 | 100 | 0.43 | 0.0002 | 0.0018 | 0.0182 |
| 213 | 8.00 | 4.00 | 100.00 | 0.00 | 0.00 | 0.00 | 0.00 | 0.00 | 100 | 0.3 | 0.0002 | 0.0019 | 0.0185 |
| 17 | 8.00 | 4.00 | 61.01 | 0.00 | 0.98 | 4.05 | 0.00 | 33.96 | 100 | 0.437 | 0.0003 | 0.0027 | 0.0269 |
| 374 | 7.55 | 2.74 | 0.00 | 0.00 | 0.00 | 0.00 | 23.04 | 76.96 | 100 | 0.692 | 0.0003 | 0.0029 | 0.0292 |
| 199 | 10.87 | 5.58 | 75.67 | 0.00 | 0.00 | 0.00 | 0.00 | 24.33 | 100 | 0.373 | 0.0003 | 0.0032 | 0.0321 |
| ... | ... | ... | ... | ... | ... | ... | ... | ... | ... | ... | ... | ... | ... |
| 318 | 325.33 | 3553.01 | 32.46 | 29.37 | 2.08 | 4.81 | 11.58 | 19.70 | 100 | 0.694 | 0.3801 | 3.8014 | 38.0143 |
| 372 | 395.70 | 3598.36 | 25.95 | 31.21 | 0.00 | 6.55 | 12.34 | 23.91 | 100 | 0.722 | 0.4005 | 4.0053 | 40.0528 |
| 115 | 409.63 | 3414.97 | 14.08 | 16.26 | 21.22 | 5.77 | 21.70 | 20.98 | 100 | 0.818 | 0.4307 | 4.3066 | 43.0656 |
| 279 | 451.17 | 5638.71 | 18.86 | 24.11 | 0.79 | 5.46 | 35.22 | 15.56 | 100 | 0.806 | 0.6007 | 6.0066 | 60.0656 |
| 22 | 1342.18 | 10862.95 | 14.54 | 20.08 | 8.21 | 4.71 | 18.46 | 34.00 | 100 | 0.762 | 1.2761 | 12.7613 | 127.6126 |
| 419 | 850.28 | 10910.92 | 0.08 | 41.37 | 7.72 | 7.68 | 31.68 | 11.47 | 100 | 0.954 | 1.6047 | 16.0472 | 160.4723 |

*Table 10: Runoff 2 - 0%*

| Street Inle | Area | Vegetated A | Streets Cla | Trees | Buildings | Streets | Build Class | Total | C | Q (2 mm/h) [L/s] | Q (20 mm/h) [L/s] | Q (200 mm/h) [L/s] |
|---|---|---|---|---|---|---|---|---|---|---|---|---|
| 204 | 2.7 | 0.0 | 0.0 | 100.0 | 0.0 | 0.0 | 0.0 | 100 | 0.3 | 0.0001 | 0.0013 | 0.0127 |
| 89 | 2.7 | 0.0 | 0.0 | 81.5 | 0.0 | 18.5 | 0.0 | 100 | 0.43 | 0.0002 | 0.0018 | 0.0182 |
| 213 | 4.0 | 0.0 | 0.0 | 100.0 | 0.0 | 0.0 | 0.0 | 100 | 0.3 | 0.0002 | 0.0019 | 0.0185 |
| 374 | 2.7 | 77.0 | 23.0 | 0.0 | 0.0 | 0.0 | 0.0 | 100 | 0.692 | 0.0003 | 0.0029 | 0.0292 |
| 199 | 5.6 | 24.3 | 0.0 | 75.7 | 0.0 | 0.0 | 0.0 | 100 | 0.373 | 0.0003 | 0.0032 | 0.0321 |
| 15 | 2.7 | 0.0 | 0.0 | 0.0 | 0.0 | 100.0 | 0.0 | 100 | 1 | 0.0004 | 0.0042 | 0.0422 |
| ... | ... | ... | ... | ... | ... | ... | ... | ... | ... | ... | ... | ... |
| 372 | 3597.2 | 23.9 | 12.3 | 26.0 | 31.2 | 0.0 | 6.5 | 100 | 0.722 | 0.4004 | 4.0039 | 40.0393 |
| 115 | 4.0 | 0.0 | 0.0 | 99.8 | 0.0 | 0.2 | 0.0 | 100 | 0.301 | 0.4303 | 4.3034 | 43.0337 |
| 246 | 1450.5 | 22.5 | 15.6 | 8.4 | 46.4 | 2.1 | 5.0 | 100 | 0.852 | 0.5600 | 5.6000 | 56.0000 |
| 279 | 5640.8 | 15.6 | 35.2 | 18.8 | 24.1 | 0.8 | 5.5 | 100 | 0.806 | 0.6009 | 6.0091 | 60.0913 |
| 22 | 12484.4 | 31.8 | 18.9 | 13.2 | 23.4 | 7.4 | 5.3 | 100 | 0.781 | 1.2032 | 12.0317 | 120.3171 |
| 419 | 10910.9 | 11.5 | 31.7 | 0.1 | 41.4 | 7.7 | 7.7 | 100 | 0.954 | 1.6047 | 16.0472 | 160.4723 |

*Table 9: Runoff 2 - 10%*

| Street Inle | Area | Build Class. | Streets Class. | Vegetated Areas Class. | Buildings | Streets | Trees | Tot | C | Q (2 mm/h) [L/s] | Q (20 mm/h) [L/s] | Q (200 mm/h) [L/s] |
|---|---|---|---|---|---|---|---|---|---|---|---|---|
| 83 | 2.7 | 0.0 | 0.0 | 0.0 | 0.0 | 100.0 | 0.0 | 100 | 1 | 0.00042 | 0.00422 | 0.04222 |
| 106 | 2.7 | 7.9 | 92.0 | 0.1 | 0.0 | 0.0 | 0.0 | 100 | 1 | 0.00042 | 0.00422 | 0.04222 |
| 15 | 2.7 | 0.0 | 0.0 | 0.0 | 0.0 | 100.0 | 0.0 | 100 | 1 | 0.00042 | 0.00422 | 0.04222 |
| 327 | 5.5 | 10.2 | 44.7 | 45.1 | 0.0 | 0.0 | 0.0 | 100 | 0.82 | 0.00069 | 0.00690 | 0.06904 |
| 86 | 5.4 | 7.5 | 70.0 | 22.4 | 0.0 | 0.0 | 0.0 | 100 | 0.91 | 0.00076 | 0.00757 | 0.07575 |
| 367 | 5.5 | 3.3 | 95.8 | 0.9 | 0.0 | 0.0 | 0.0 | 100 | 0.996 | 0.00084 | 0.00839 | 0.08386 |
| ... | ... | ... | ... | ... | ... | ... | ... | ... | ... | ... | ... | ... |
| 131 | 3448.2 | 1.8 | 19.4 | 14.3 | 41.3 | 11.9 | 11.4 | 100 | 0.863 | 0.45877 | 4.58772 | 45.87721 |
| 104 | 128.6 | 10.6 | 39.6 | 42.0 | 0.0 | 2.0 | 5.8 | 100 | 0.791 | 0.52168 | 5.21682 | 52.16816 |
| 198 | 5671.9 | 5.4 | 35.4 | 15.7 | 23.9 | 0.8 | 18.8 | 100 | 0.806 | 0.80478 | 8.04785 | 80.47846 |
| 211 | 7330.1 | 2.5 | 18.9 | 34.2 | 33.8 | 0.7 | 10.0 | 100 | 0.793 | 0.99613 | 9.96133 | 99.61330 |
| 22 | 11620.0 | 4.7 | 18.0 | 32.8 | 19.5 | 11.3 | 13.7 | 100 | 0.773 | 1.38476 | 13.84759 | 138.47591 |
| 419 | 11190.4 | 7.6 | 31.1 | 11.3 | 40.4 | 9.0 | 0.6 | 100 | 0.951 | 1.64065 | 16.40654 | 164.06539 |

*Table 11: Runoff 2 - 50%*

The average runoff for all three clogging scenarios has been calculated across all three precipitation scenarios. Consistently, it has been observed that the scenario with the highest clogging percentage exhibits higher runoff compared to scenarios with lower clogging percentages within all intensity cases.

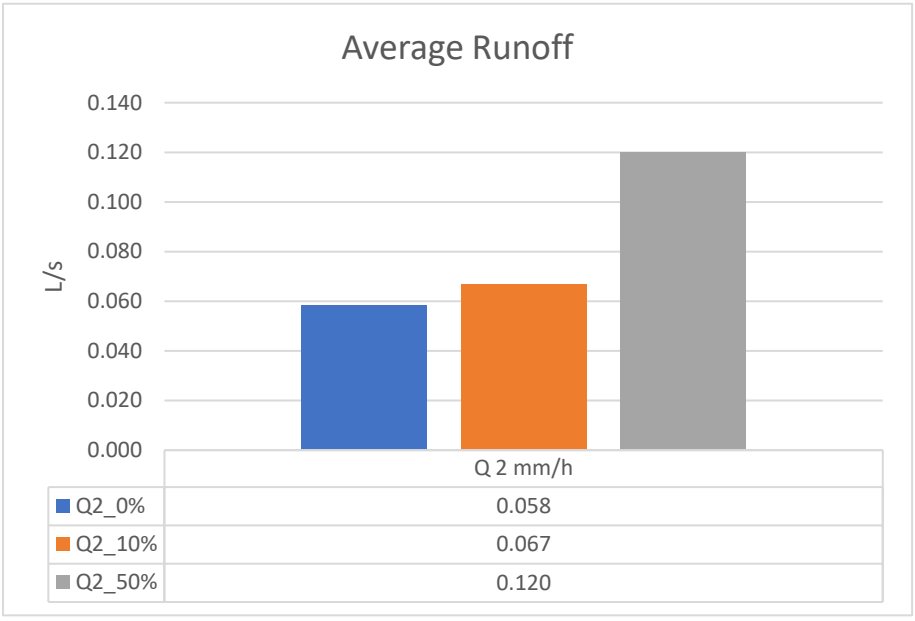


*Figure 37: Average Runoff in the 2mm/h scenario*

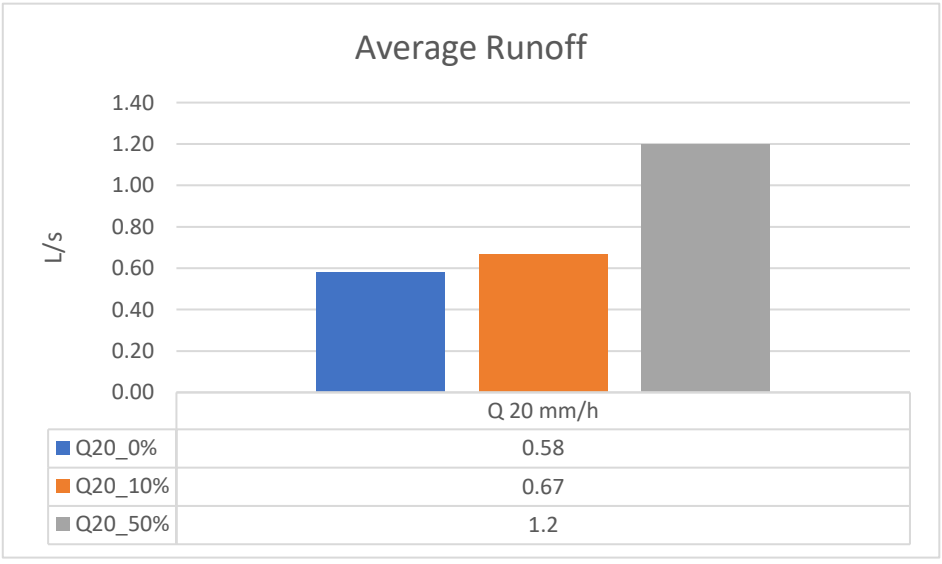


*Figure 38: Average Runoff in the 20 mm/h scenario*

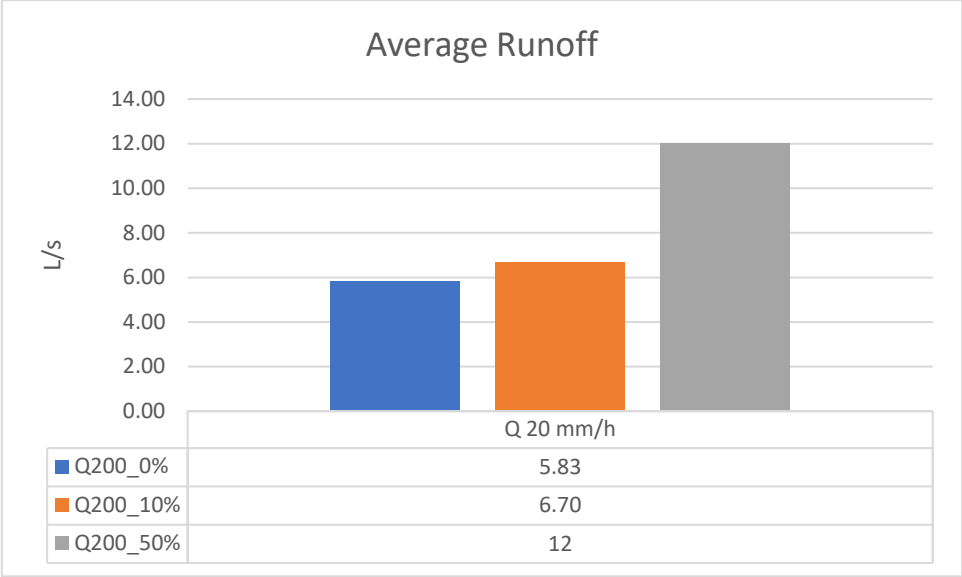


*Figure 39: Average Runoff in the 200 mm/h scenario*

Repeating the logarithmic plots to assess any potential discrepancies, similarly to Workflow 1, the logarithmic plots have been regenerated. As a result, it appears that the observed discrepancy is negligible across all precipitation scenarios.

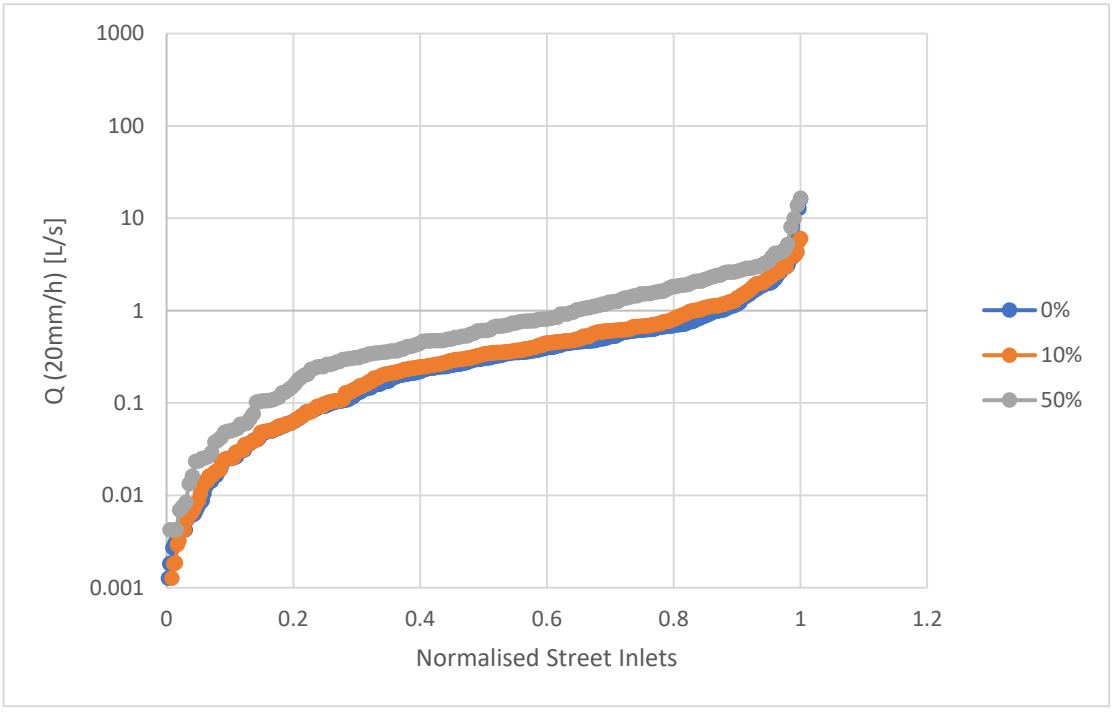


*Figure 40: Water Volume Intake for the street inlets in each scenario (20 mm/h)*

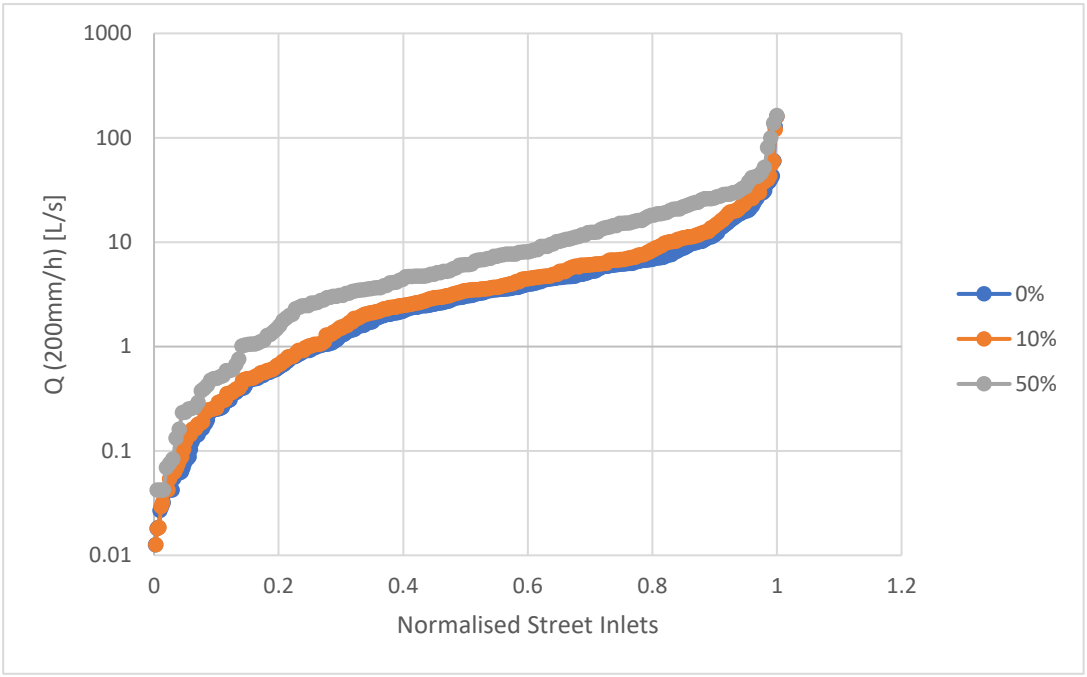


*Figure 41: Water Volume Intake for the street inlets in each scenario (200 mm/h)*

To quantify potential discrepancies within this workflow, scatter plots were generated where every blue point represents a street inlet in common analysed. In the scenario with 10% clogging, it was observed that approximately 5% of street inlets considered, were expected to receive less runoff when clogged. In the scenario with 50% clogging, this percentage increased slightly to approximately 6%. These numbers, compared to those obtained in the first workflow, are significantly smaller, contributing to much more accurate results. The presence of this remaining discrepancy might be attributed to the watershed delineation algorithm used in ArcGIS Pro.

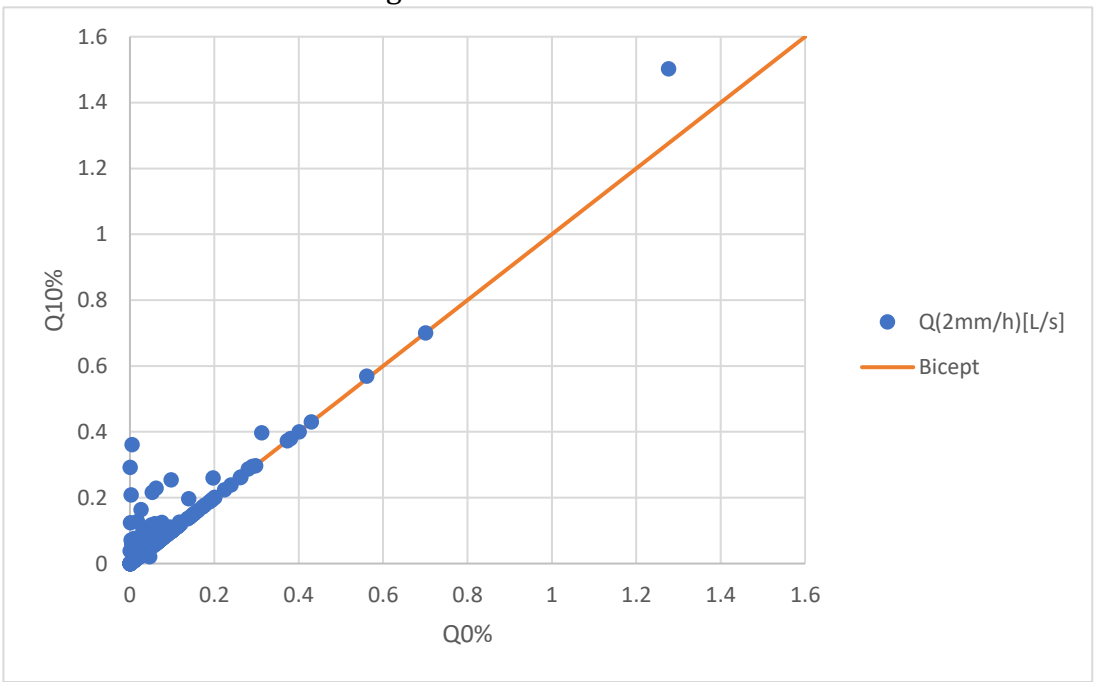


*Figure 42: Scatter Plot – Discrepancy Quantification between scenarios 0% and 10%*

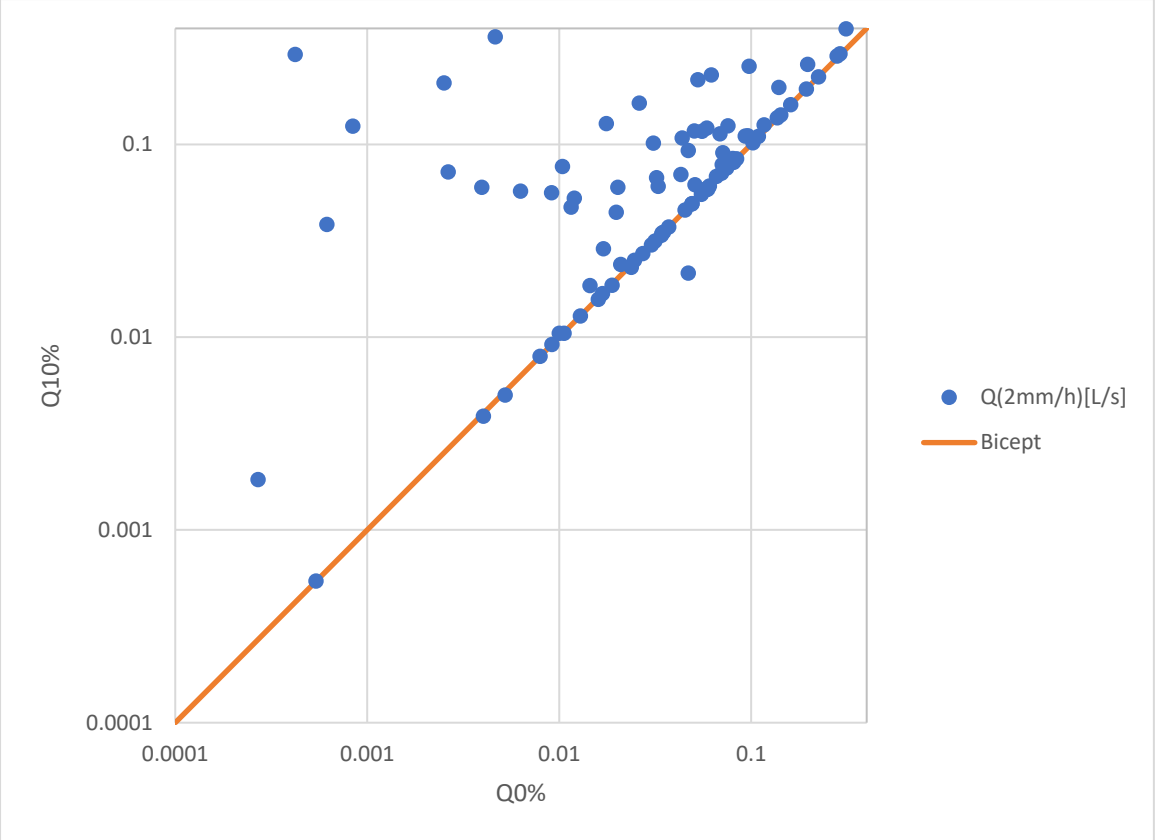


*Figure 43: Scatter Plot – Discrepancy Quantification between scenarios 0% and 10% - Log Scale*

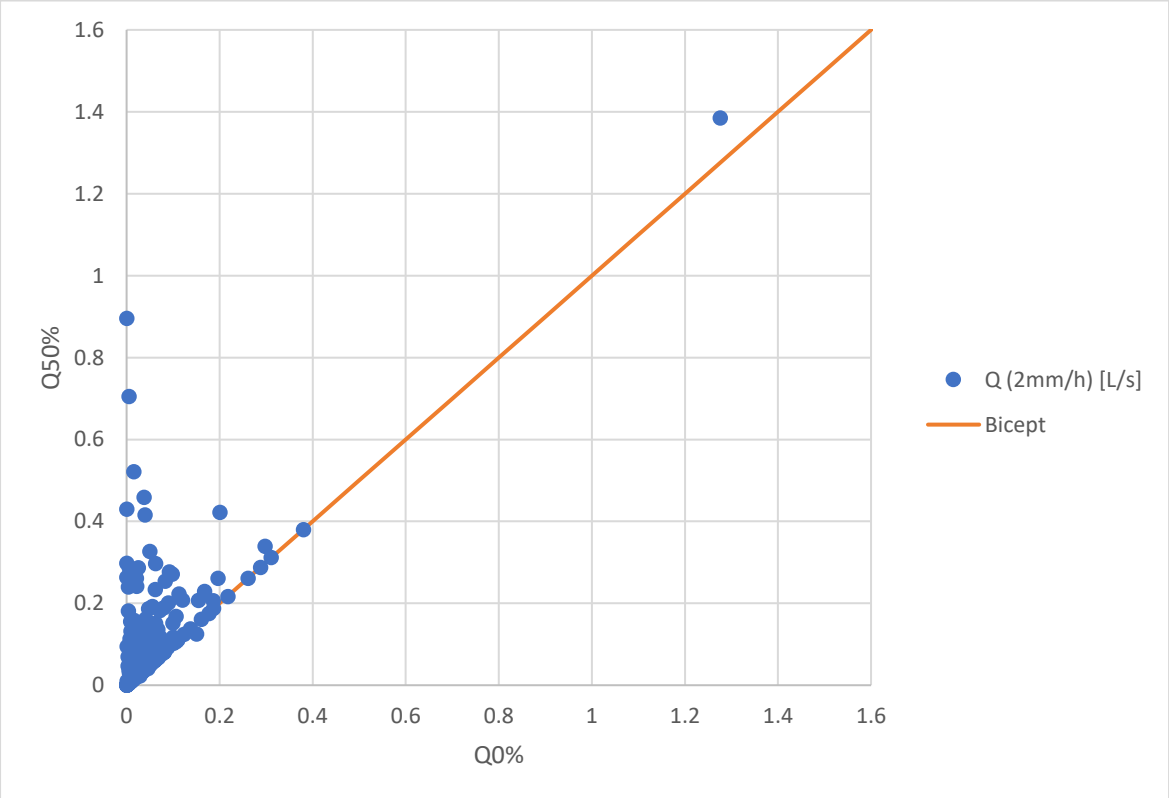


*Figure 44: Scatter Plot – Discrepancy Quantification between scenarios 0% and 50%*

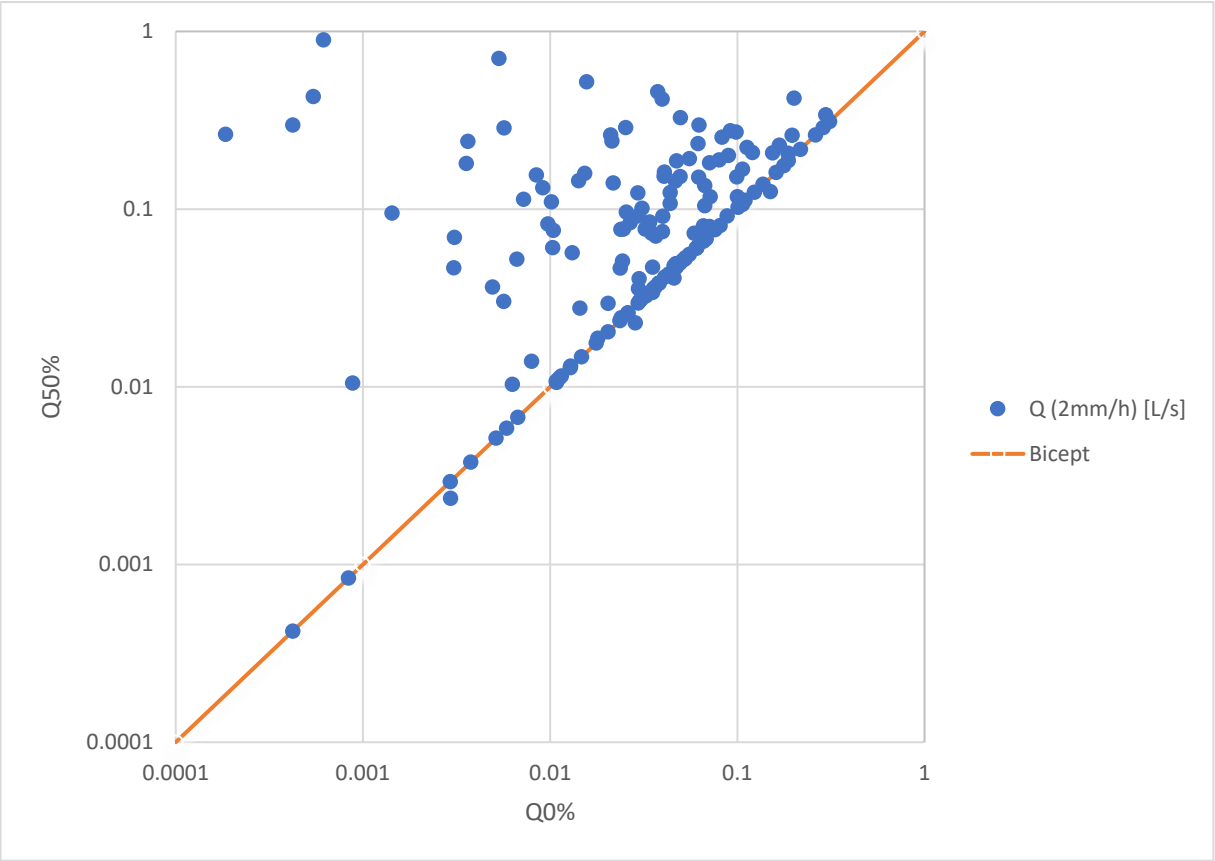


*Figure 45: Scatter Plot – Discrepancy Quantification between scenarios 0% and 50% - Log Scale*

In this final section of the results obtained, the focus shifts on assessing the risk associated with street inlets, particularly in relation to their flow capacity. Street inlets have a critical role in urban drainage systems, as they are crucial in collecting surface runoff and direct it into the stormwater network. However, understanding the limitations of these inlets is fundamental for an effective urban flood management[19].

Due to the lack of data regarding the specific dimensions for the street inlets under study, the estimation of their flow interception capacity has been assigned equal to 10 l/s. This value was selected based on the available literature and experimental studies. However, it's important to acknowledge the uncertainty associated with this consideration. Street inlet dimensions can vary significantly depending on factors such as location, design standards, and surrounding infrastructure[21]. Therefore, while the chosen value of 10 l/s provides a reasonable estimate, it's important to recognize the uncertainty in interpreting the results.

In the tables below the number of street inlets that exceeded the threshold of 10 l/s, have been reported.

| Scenario | 0% | 10% | 50% |
|---|---|---|---|
| Rainfall Intensity | Number of street inlets at risk | | |
| 2 mm/h | 0 | 0 | 0 |
| 20 mm/h | 2 | 2 | 3 |
| 200 mm/h | 53 | 63 | 71 |

*Table 12: Number of street inlets under risk*

In the tables below the street inlets expected to flood in each scenario are reported:

| Scenario | 0% |
|---|---|
| Rainfall Intensity | Street Inlet ID |
| 2 mm/h | - |
| 20 mm/h | 22, 419 |
| 200 mm/h | 20,27,120,291,424,110,415,277,122,320,34,324,178,61,64,19,185,262,215,243,153,105,420,334,7,352,246,378,296,370,42,134,128,10,102,369,73,244,350,124,432,96,150,273,126,429,389,318,372,115,279,22,419 |

| Scenario | 10% |
|---|---|
| Rainfall Intensity | Street Inlet ID |
| 2 mm/h | - |
| 20 mm/h | 22, 419 |
| 200 mm/h | 20,27,163,120,291,424,110,363,415,161,81,277,122,320,264,34,392,270,178,174,60,179,324,201,64,19,262,215,243,153,105,380,7,352,296,370,42,185,128,10,93,65,73,333,244,52,134,350,124,432,87,150,273,130,389,318,126,372,115,246,279,22,419 |

| Scenario | 50% |
|---|---|
| Rainfall Intensity | Street Inlet ID |
| 2 mm/h | - |
| 20 mm/h | 22, 211, 419 |
| 200 mm/h | 163,27,125,424,363,219,320,297,348,20,284,362,61,243,225,98,19,322,253,355,118,108,414,143,78,141,105,173,110,352,171,166,35,296,290,392,221,378,153,178,369,122,334,280,160,62,49,134,350,256,213,172,148,263,123,432,72,87,126,147,273,318,388,128,373,131,104,198,211,22,419 |

*Table 13:Street Inlets ID*

In the next figures, an example of how a sub catchment area associated to a street inlet (**98**), changes due to the blocking of a street inlet in the near proximity (**102**).


*Figure 46: Initial sub catchment area associated to the street inlet 98 (0% scenario)*


*Figure 47: Final sub catchment area associated to the street inlet 98 (50% scenario)*

For visualizing the number and location of these inlets in all scenarios, six maps have been generated and are provided below:

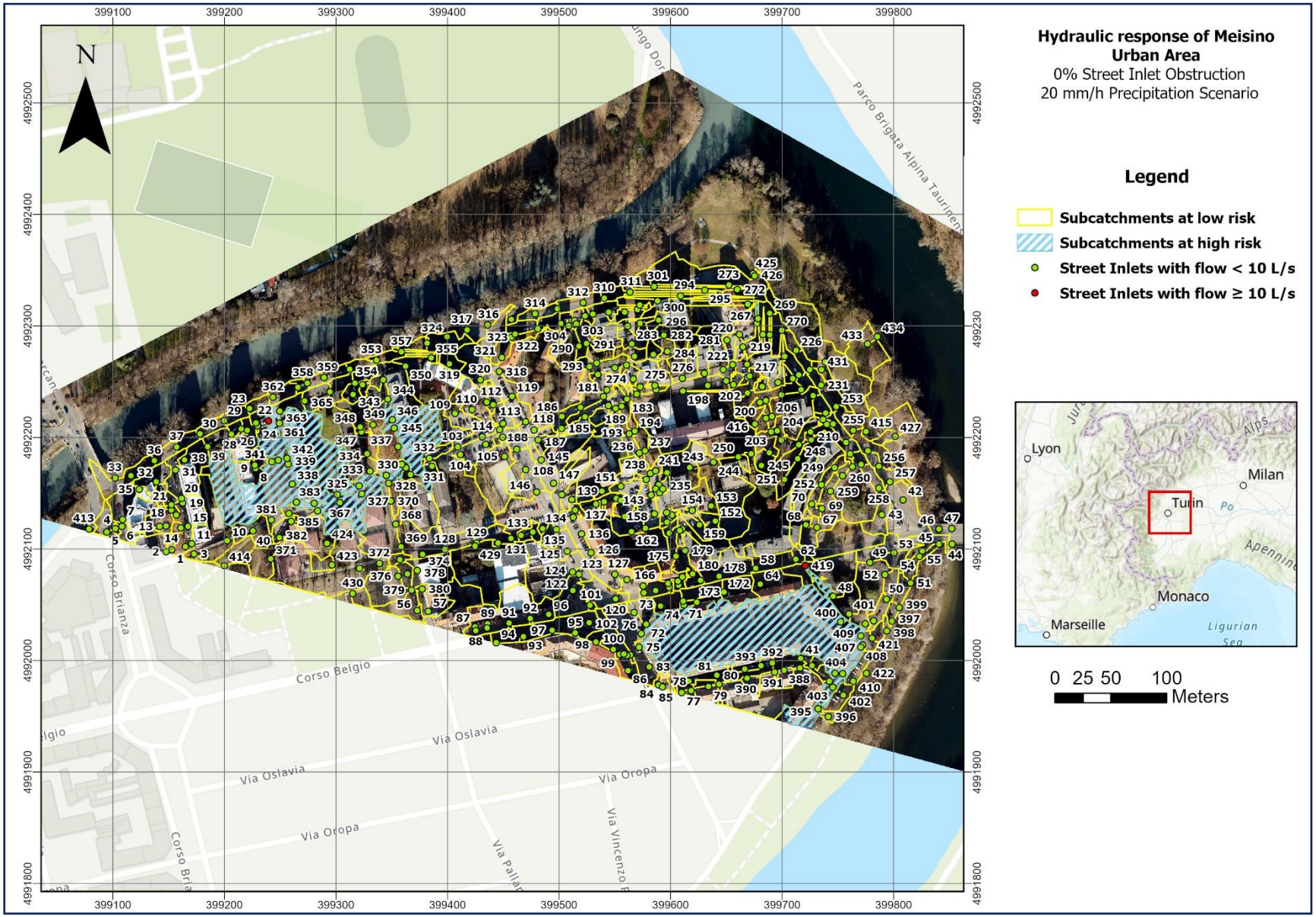
Hydraulic response of Meisino Urban Area
0% Street Inlet Obstruction
20 mm/h Precipitation Scenario
Legend
Subcatchments at low risk
Subcatchments at high risk
Street Inlets with flow < 10 L/s
Street Inlets with flow ≥ 10 L/s
N
Corso Belgio
Via Oslavia
Via Oropa
Corso Brianza
Via Vincenzo
Parco Brigata Alpina Taurinense
Lyon
Milan
Turin
Po
Alps
Apennine
Monaco
Marseille
Ligurian Sea
0 25 50 100
Meters

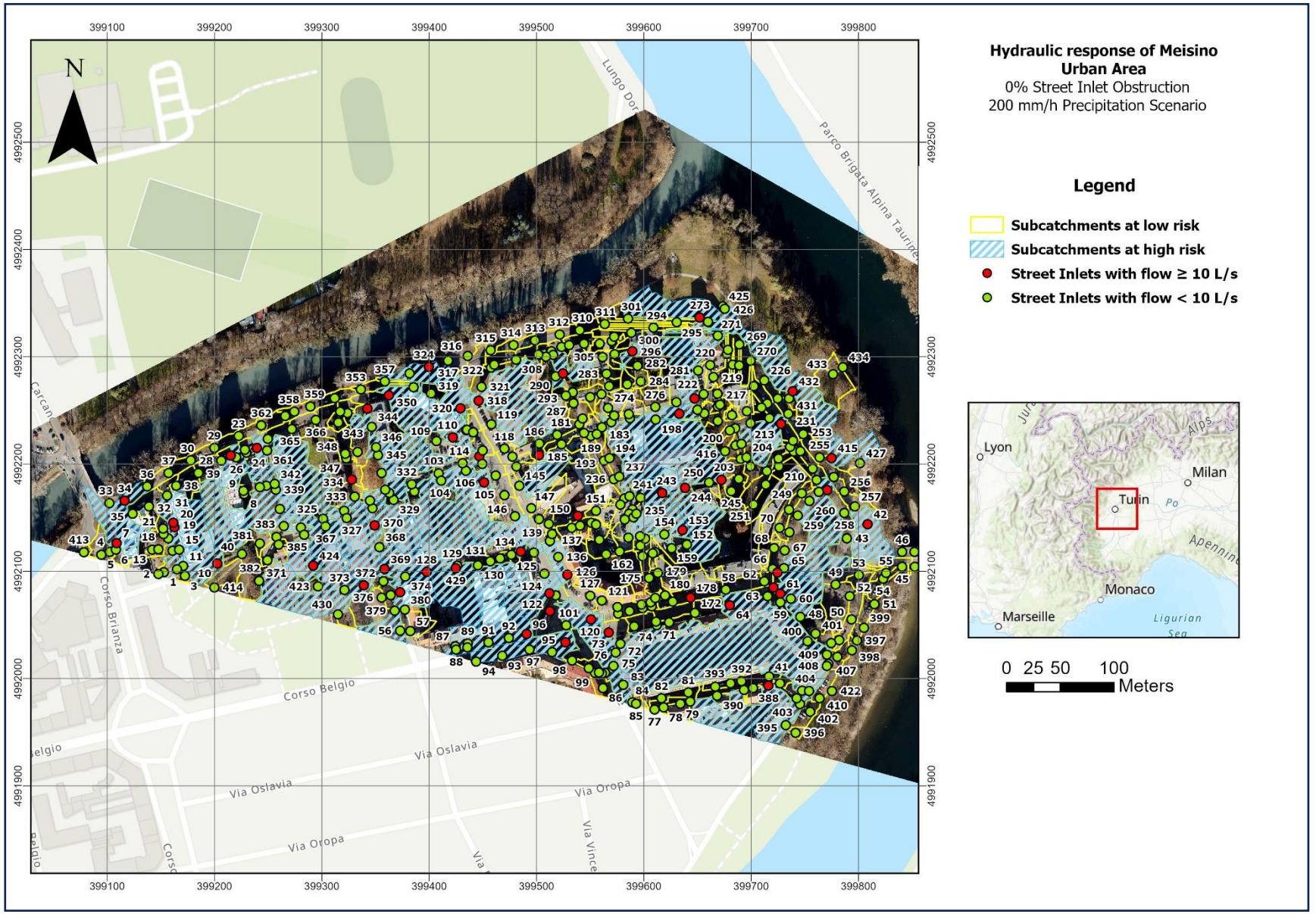
Hydraulic response of Meisino Urban Area
0% Street Inlet Obstruction
200 mm/h Precipitation Scenario
Legend
Subcatchments at low risk
Subcatchments at high risk
Street Inlets with flow ≥ 10 L/s
Street Inlets with flow < 10 L/s
N
399100
399200
399300
399400
399500
399600
399700
399800
4992500
4992400
4992300
4992200
4992100
4992000
4991900
Corso Belgio
Via Oslavia
Via Oropa
Corso Brianza
Parco Brigata Alpina Taurinense
Lungo Dora
Lyon
Milan
Turin
Po
Alps
Apennine
Monaco
Marseille
Ligurian Sea
0 25 50 100
Meters

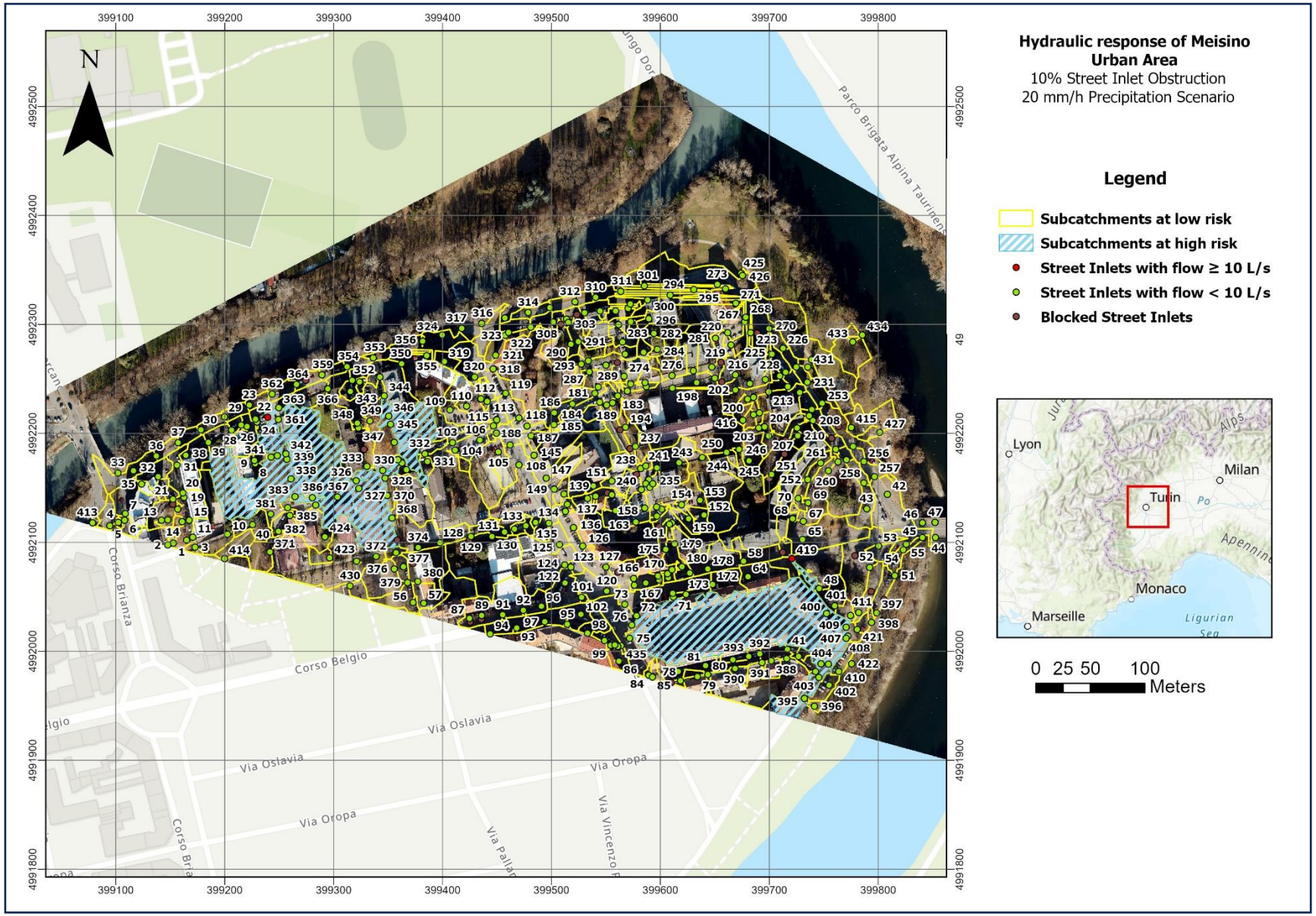
Hydraulic response of Meisino Urban Area
10% Street Inlet Obstruction
20 mm/h Precipitation Scenario
Legend
Subcatchments at low risk
Subcatchments at high risk
Street Inlets with flow ≥ 10 L/s
Street Inlets with flow < 10 L/s
Blocked Street Inlets
N
Corso Brianza
Corso Belgio
Via Oslavia
Via Oropa
Via Vincenzo
Parco Brigata Alpina Taurinense
Lyon
Milan
Turin
Monaco
Marseille
Alps
Po
Apennine
Ligurian Sea
0 25 50 100
Meters

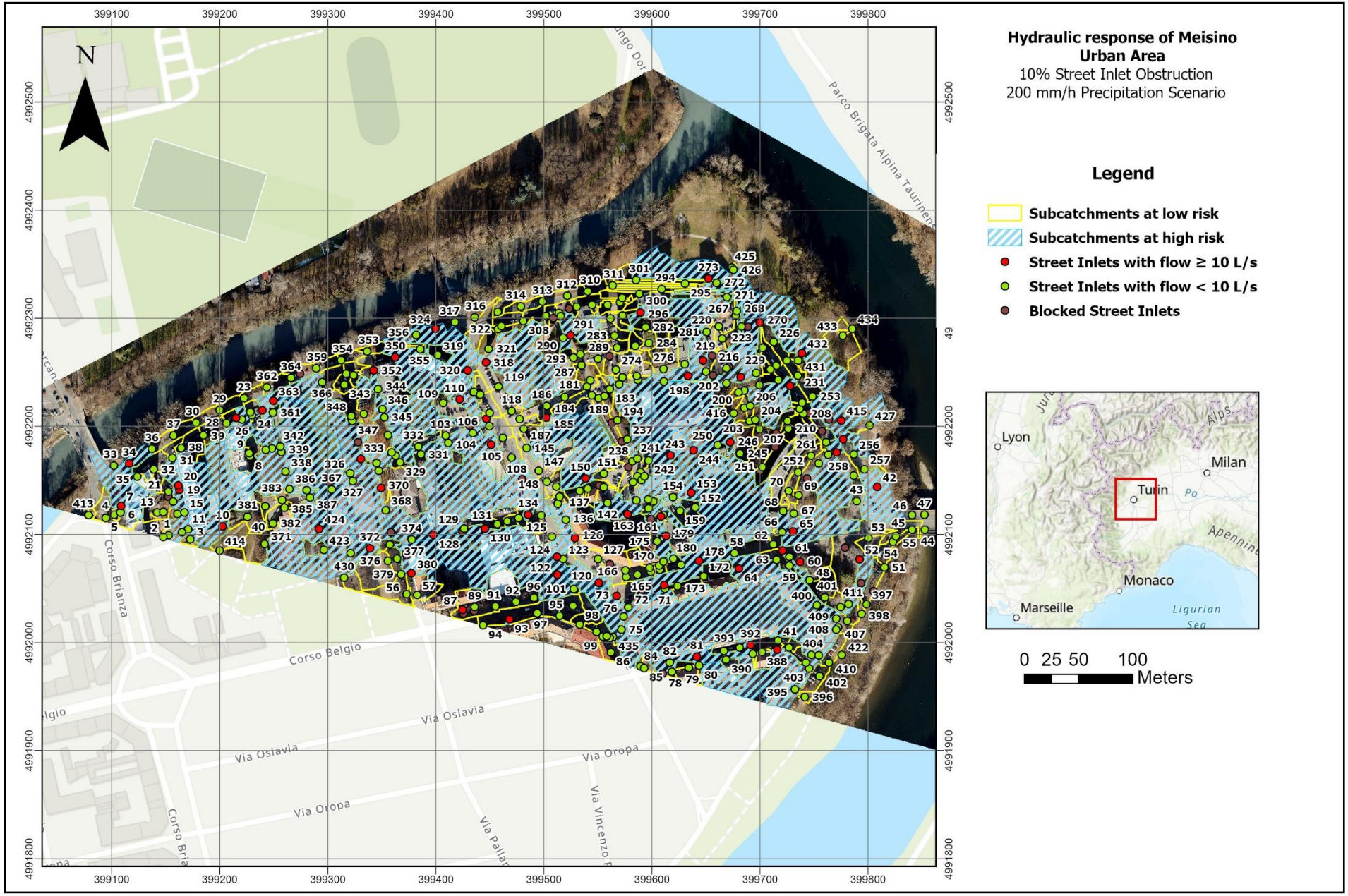
Hydraulic response of Meisino Urban Area
10% Street Inlet Obstruction
200 mm/h Precipitation Scenario
Legend
Subcatchments at low risk
Subcatchments at high risk
Street Inlets with flow ≥ 10 L/s
Street Inlets with flow < 10 L/s
Blocked Street Inlets
N
399100
399200
399300
399400
399500
399600
399700
399800
4992500
4992400
4992300
4992200
4992100
4992000
4991900
4991800
Corso Brianza
Corso Belgio
Via Oslavia
Via Oropa
Via Vincenzo
Parco Brigata Alpina Taurinense
Lyon
Milan
Turin
Po
Alps
Apennine
Monaco
Marseille
Ligurian Sea
0 25 50 100
Meters

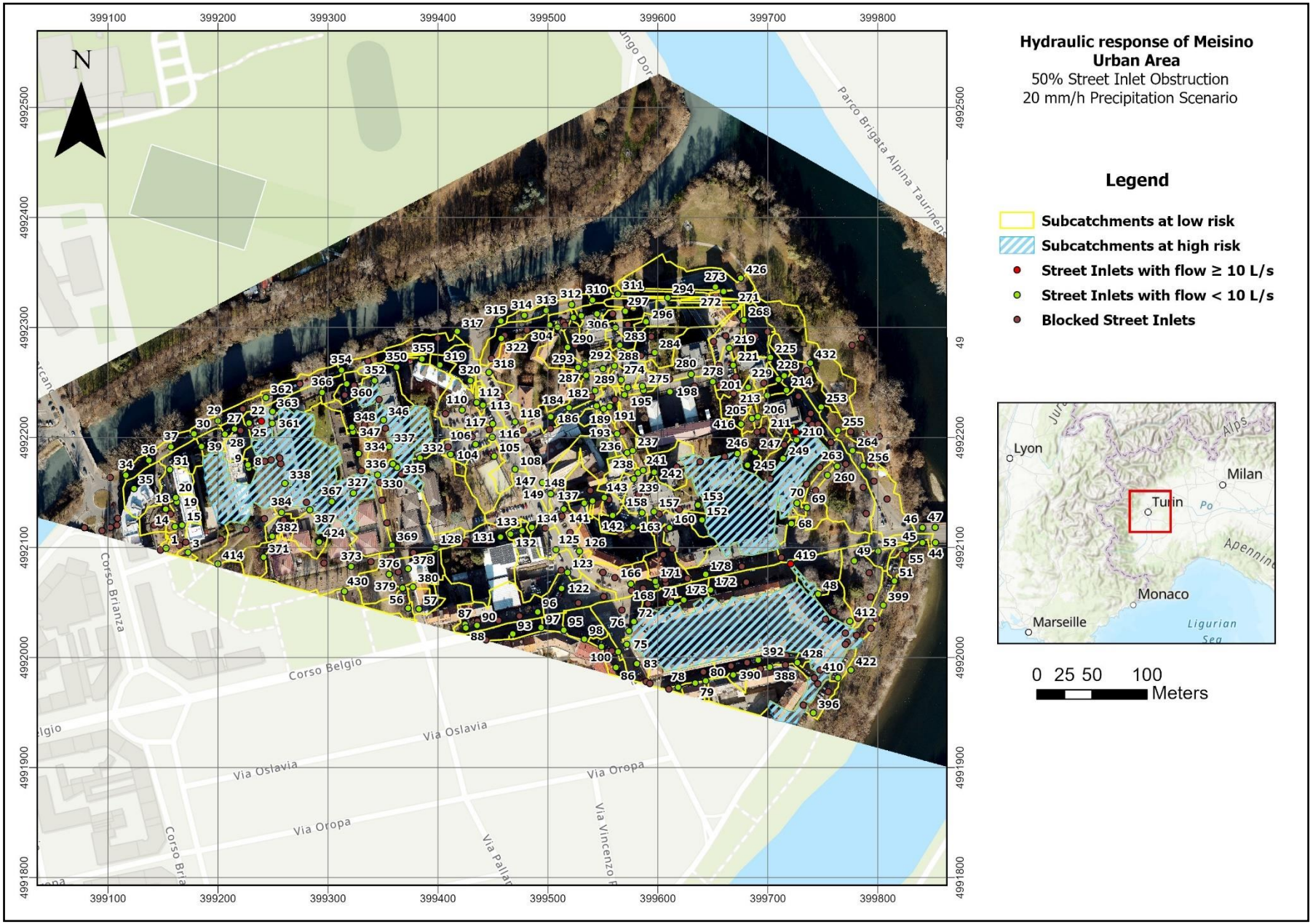
Hydraulic response of Meisino Urban Area
50% Street Inlet Obstruction
20 mm/h Precipitation Scenario
Legend
Subcatchments at low risk
Subcatchments at high risk
Street Inlets with flow ≥ 10 L/s
Street Inlets with flow < 10 L/s
Blocked Street Inlets
N
399100
399200
399300
399400
399500
399600
399700
399800
4992500
4992400
4992300
4992200
4992100
4992000
4991900
4991800
Corso Brianza
Corso Belgio
Via Oslavia
Via Oropa
Via Vincenzo
Parco Brigata Alpina Taurinense
Lyon
Milan
Turin
Po
Alps
Apennine
Monaco
Marseille
Ligurian Sea
0 25 50 100
Meters

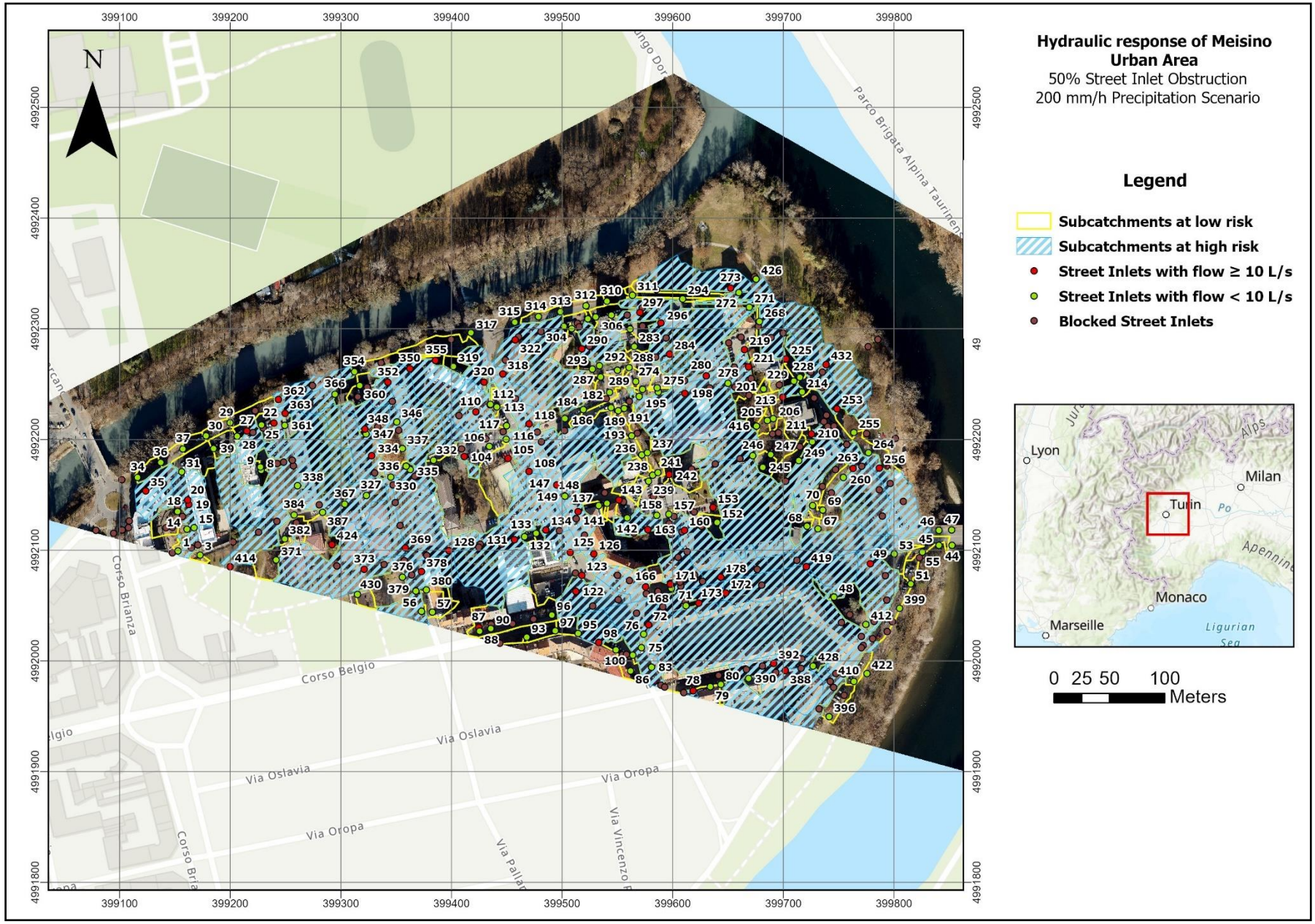
Hydraulic response of Meisino Urban Area
50% Street Inlet Obstruction
200 mm/h Precipitation Scenario
Legend
Subcatchments at low risk
Subcatchments at high risk
Street Inlets with flow ≥ 10 L/s
Street Inlets with flow < 10 L/s
Blocked Street Inlets
N
399100
399200
399300
399400
399500
399600
399700
399800
4992500
4992400
4992300
4992200
4992100
4992000
4991900
4991800
Corso Briana
Corso Belgio
Via Oslavia
Via Oropa
Via Vincenzo
Parco Brigata Alpina Taurinense
Lyon
Milan
Turin
Po
Alps
Apennine
Monaco
Marseille
Ligurian Sea
0 25 50 100
Meters

## 4.4 Hydrological Analysis – Analysis on DSM

In this section, there has been an attempt to use a DSM (Digital Surface Model) as an alternative approach for generating sub catchments, following Workflow 2. The idea behind using a DSM instead of a DTM for flooding analysis was to get a more comprehensive perspective of flood dynamics by considering the features present on the surface. However, several challenges during the analysis have been encountered since numerous gaps appeared during the 'Watershed Delineation' process. These gaps would have influenced even more the overall accuracy of the study leading to more uncertainties.

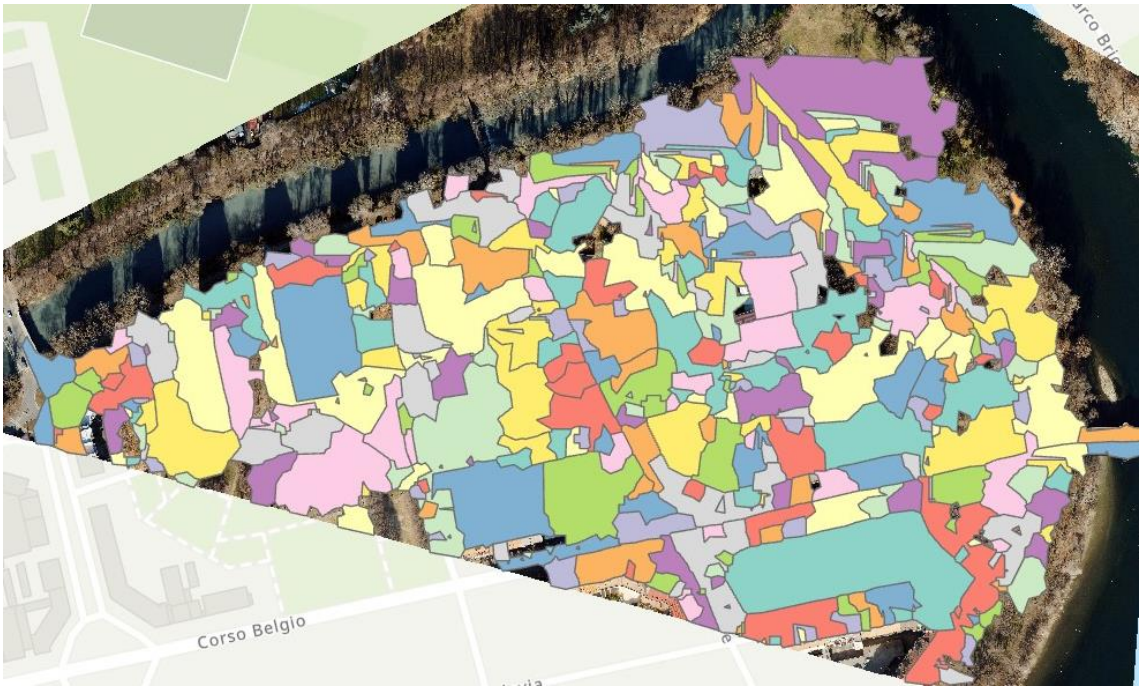


*Figure 318: Watershed Delineation - DSM*

## 4.5 Limitations and Uncertainties

Selecting the most suitable modelling workflow can be a considerable challenge, particularly given the complexity of hydrological systems, especially within urban environments. The case study shows that GIS techniques can identify the most vulnerable areas under a quick scan of the area. They provide a first insight, and they are an easy and fast alternative to assess flood risks and to analyse the effect of possible mitigation measures. Though different uncertainties may arise:

1. Firstly, the generation of watersheds using ArcGIS Pro may introduce potential inaccuracies or simplifications in polygon delineation. While this process facilitates watershed delineation, it may result in oversimplified representations of the sub catchments.

2. The initial approach (Workflow 1) produced inaccurate results, which led to a non-conventional methodology for watershed delineation. Although this second approach produced more reasonable results, uncertainties remain regarding its reliability.

3. The Hydrological Analysis has been implemented only for a small portion of the original Digital Terrain Model (DTM) due to limited availability on hydrological data. Consequently, the delineation of watersheds may be influenced by this limitation.

4. The absence of data on street inlet dimensions limits the precision of the risk assessment for each inlet. Consequently, the approach may not fully capture potential flood risks associated with street inlets.

5. The use of the Digital Terrain Model instead of the Digital Surface Model may introduce limitations as it overlooks elevations regarding surface elements that could impact flood dynamics, potentially affecting the accuracy of the analysis.

# 5 Conclusions

This thesis has explored the application of two simplified GIS-based flood models to assess potential flood phenomena resulting from extreme rainfall events. The increasing frequency of extreme rainfall events, attributed to climate change, presents significant challenges for urban areas worldwide. In response to these challenges, this study highlights the importance of using advanced technologies such as LiDAR data at high-resolution, and Digital Elevation Models (DEMs). These tools offer valuable information regarding surface topography that can be extremely helpful in the context of hydrological processes, and flood risk assessment. Therefore, they can be fundamental in urban flood management.

In order to identify the best approach, different methodologies have been studied along the way in order to find a solution that while simplified, it would have produced accurate results. Initially, the detailed study of the roads has been considered a fundamental input for the flood modelling. However, the required inputs for ArcHydro tools have changed the analysis towards a less detailed approach.

Despite the less detailed approach, the followed workflow demonstrated the potential of such methodologies in assessing the response of urban areas to extreme precipitation events and their impact on the street inlets. Specifically, the study highlights the link between street inlet clogging and flooding events, demonstrating the cumulative effects across multiple inlets. The findings revealed an increase in flood-prone street inlets, particularly notable in scenarios of 10% clogging under a 20mm/h rainfall intensity, peaking in the 50% scenario under the 200mm/h rainfall intensity scenario.

Acknowledging the limitations and uncertainties, this study provides a comprehensive overview of the issue and its potential impacts. It highlights the importance of regular maintenance for street inlets and emphasizes the necessity to increase their interception capacity to tackle extreme precipitations in response to climate change phenomena, and so enhanced urban adaptation strategies.

# References and Websites


1. Prevention Web, 5 Jan. 2022: https://www.preventionweb.net/news/mitigating-impact-climate-change-and-flooding-italy

2. Pluvial flood risk assessment for 2021–2050 under climate change scenarios in the Metropolitan City of Venice, 8 January 2024, Elena Allegri, Marco Zanetti, Silvia Torresan, Andrea Critto

3. Perspectives on Digital Elevation Model (DEM) Simulation for Flood Modeling in the Absence of a High-Accuracy Open Access Global DEM, 18 December 2018: https://www.frontiersin.org/articles/10.3389/feart.2018.00233/full

4. https://www.lastampa.it/torino/2020/12/05/news/salvateci-dalle-piene-del-po-alzando-gli-argini-nel-parco-del-meisino-1.39622426/, 5 December 2020

5. The Use of LiDAR-Derived DTM in Flood Applications: A Review by Nur Atirah Muhadi, Ahmad Fikri Abdullah, Siti Khairunniza Bejo, Muhammad Razif Mahadi, Ana Mijic: https://www.mdpi.com/2072-4292/12/14/2308

6. Decido Project, 2 Mar. 2023:https://decido-project.eu/turin-pilot/

7. LiDAR DTM Data for Flood Mapping and Assessment; Opportunities and Challenges: A Review by: Gizachew Kabite Wedajo, 27 Sept. 2017: https://pdfs.semanticscholar.org/49fb/a5fbc6c36b1a6791fecba0f8b8365f69c0dc.pdf

8. Breaklines in surface modelling: https://desktop.arcgis.com/en/arcmap/latest/extensions/3d-analyst/breaklines-in-surface-modeling.htm

9. Classification: https://www.nv5geospatialsoftware.com/docs/Classification.html

10. Pluvial (rain-related) flooding in urban areas: the invisible hazard, Donald Houston, Alan Werritty, David Bassett, Alistair Geddes, Andrew Hoolachan and Marion McMillan, November 2011 (page 13)

11. Characteristics and Accuracy of Large Area Covering Height Models. Int. Arch. Photogramm. Remote Sens. Spat. Inf. Sci. 2013, Jacobsen, K. XL-1/W1, 157–162:

https://www.semanticscholar.org/reader/2268c06e06aec5df49bff0b0ebc91a83741c0cc0

12. Elevation Modeling - the differences between DTM, DSM & DEM, Hellen Grace Llames, December 2022: https://support.plexearth.com/hc/en-us/articles/4642425453201-Elevation-Modeling-the-differences-between-DTM-DSM-DEM

13. How Fill works: https://pro.arcgis.com/en/pro-app/latest/tool-reference/spatial-analyst/how-fill-works.htm

14. Fill (Spatial Analyst): https://pro.arcgis.com/en/pro-app/latest/tool-reference/spatial-analyst/fill.htm

15. Flow Direction (Spatial Analyst): https://pro.arcgis.com/en/pro-app/3.1/tool-reference/spatial-analyst/flow-direction.htm

16. How Flow Accumulation works: https://pro.arcgis.com/en/pro-app/latest/tool-reference/spatial-analyst/how-flow-accumulation-works.htm

17. Snap Pour Point (Spatial Analyst): https://pro.arcgis.com/en/pro-app/latest/tool-reference/spatial-analyst/snap-pour-point.htm

18. What is ModelBuilder?https://desktop.arcgis.com/en/arcmap/latest/analyze/modelbuilder/what-is-modelbuilder.htm

19. Runoff Coefficient (C) Fact Sheet, November 2009: https://www.waterboards.ca.gov/water_issues/programs/swamp/docs/cwt/guidance/513.pdf

20. An overview of the Hydrology toolset: https://pro.arcgis.com/en/pro-app/latest/tool-reference/spatial-analyst/an-overview-of-the-hydrology-tools.htm

21. Stormwater Management Technical Guidelines, 2013 : https://www.bayside.nsw.gov.au/sites/default/files/2021-08/Part%2010%20Stormwater%20Mgmt%20Tech%20Guidelines.pdf

22. Storm Sewer Inlets: https://learn.hydrologystudio.com/stormwater-studio/knowledge-base/inlets/

# Appendix A

## Workflow 1 - ModelBuilder

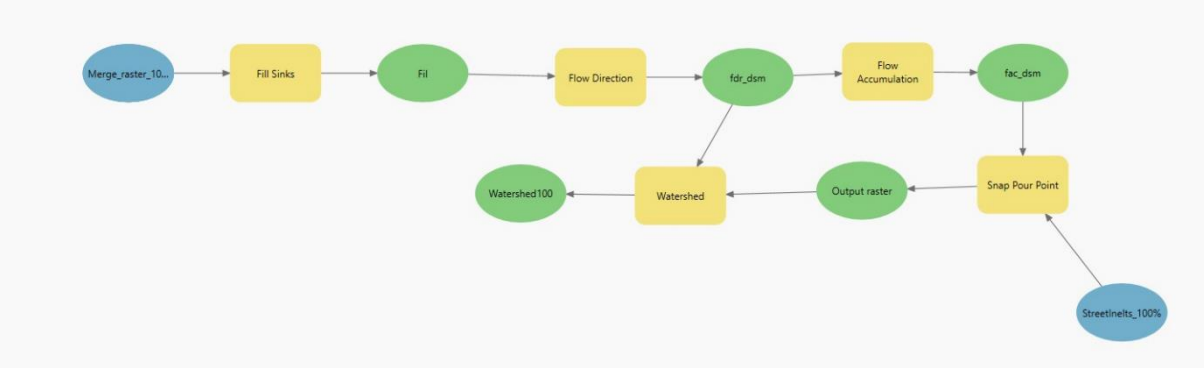


## Workflow 2 – ModelBuilder